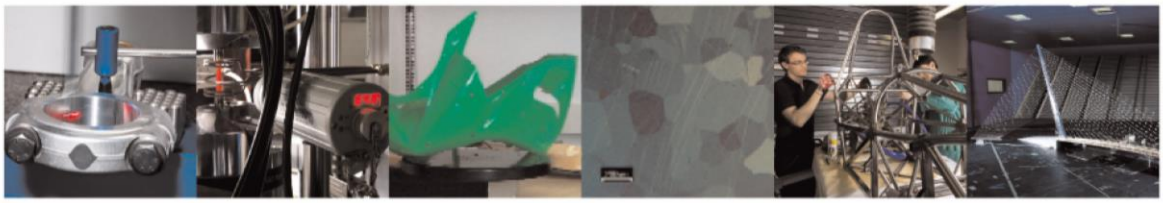

Image based statistical process monitoring via partial first order stochastic dominance

Panagiotis Tsiamyrtzis, Marco Luigi Giuseppe Grasso & Bianca Maria Colosimo

This is an Accepted Manuscript of an article published by Taylor & Francis in Quality Engineering on 03 Dec 2021, available online: https://doi.org/10.1080/08982112.2021.2008974

Image based Statistical Process Monitoring via Partial First Order Stochastic Dominance

Panagiotis Tsiamyrtzis
Department of Mechanical Engineering
Politecnico di Milano
via La Masa 1,
20156, Milan, Italy
panagiotis.tsiamyrtzis@polimi.it

Marco Luigi Giuseppe Grasso
Department of Mechanical Engineering
Politecnico di Milano
via La Masa 1,
20156, Milan, Italy
marcoluigi.grasso@polimi.it

Bianca Maria Colosimo
Department of Mechanical Engineering
Politecnico di Milano
via La Masa 1,
20156, Milan, Italy
biancamaria.colosimo@polimi.it

Abstract

The continuously evolving digitalized manufacturing industry is pushing quality engineers to face new and complex challenges. Quality data formats are evolving from simple univariate or multivariate characteristics to big data streams consisting of sequences of images and videos in the visible or infrared range; manufacturing processes are moving from series production to more and more customized applications. In this framework, novel methods are needed to monitor and keep under statistical control the process. This study presents two novel process monitoring techniques that rely on the partial first order stochastic dominance (PFOSD) concept, applicable to in-line analysis of video image data aiming at signaling out-of-control process states. Being non-parametric, they allow dealing with complex underlying dynamics and wildly varying distributions that represent the natural process conditions. A motivating case study in metal additive manufacturing is presented, where the proposed methodology enables the in-line and in-situ detection of anomalous patterns in thermal videos captured during the production of zinc samples. Performances are investigated and compared in the presence of both simulated and real data.

Key Words: Stochastic dominance, statistical process monitoring, image analysis, thermal images, additive manufacturing, laser powder bed fusion.

1 Introduction

In the field of Statistical Process Control/Monitoring (SPC/M) a process (industrial or not) under study is scrutinized, aiming to identify whether it acts under statistical stability or not. The traditional framework involves chronologically ordered quality characteristics (categorical/numerical, discrete/continuous, univariate/multivariate) measured on different products that come out from the process under study. Moving to novel manufacturing paradigms, like Additive Manufacturing (AM), the aforementioned framework may be not valid anymore, as new paradigms allow moving from mass production to one-of-a-kind and highly customized products, whose quality needs to be assessed continuously. As such products are built layer by layer, we transfer our interest of quality stability from being constant over several products to be stable over a single product/process. To this aim, the layer-wise production methodology entailed in AM becomes an enabler of a novel way to gather measurements about the process stability, while the part is being built. Indeed, machine vision systems can be used to "look" at the part in each layer but also to capture fast and transient phenomena, while the layer is being melted and solidified. This results into the capability of identifying anomalies and out-of-control (OOC) states in-situ and in-line, enabling the detection of possible defects and, when possible, the activation of in-line defect mitigation or corrective actions (Colosimo et al., 2018; Grasso and Colosimo, 2017; Everton et al., 2016).

Highly customized production has another consequence regarding the standard SPC/M philosophy. Precisely, when dealing with multiple identical items from a process, we use a phase I/II separation, where we learn some reference behavior while in phase I and test against it, in an in-line fashion, during phase II. With highly customized products though, we lack the ability of establishing such a reference or, in other words, we have a dynamically changing reference. In-situ and in-line process monitoring by means of image and video image data shall then be combined with a novel way of designing the control charts used to automatically signal any departure from a natural, but dynamically changing, behavior.

Image based SPC/M methodologies have been applied in the past. A review on this topic can be found in Megahed et. al. (2011), while some more recent works have been devoted to various (typically industrial but not only) problems as in Megahed et. al. (2012), Prats-Montalbán and Ferrer (2014), Yan et al. (2015), He et al. (2016), Kan et al.(2017), Kooshaet al. (2017) and Menafoglio et al. (2018).

All the studies mentioned above, and the mainstream literature cited therein, focus on SPC/M for image data, where single images of the same object are sequentially analyzed over time. However, in-line process monitoring frequently involves video image data, which are not just a sequence of images, as they capture process patterns that dynamically change from frame to frame. Thus, SPC/M for video image data implies that the out-of-control state translates into a perturbation of the underlying signature and only few methods have been explored and proposed in the literature like Yan et al. (2020) Colosimo and Grasso (2019), Yan et al. (2015).

One way to deal with complex and dynamic patterns in image and video-image data consists of modeling the inherent spatial or spatio-temporal structure representative of the IC process behavior. Examples of methods belonging to this stream of research include Yan et al. (2015, 2020), Megahed et al. (2012), Bui and Apley (2018), Qiu and Sun, (2007). The modeling step entailed in these methods makes them suitable to capture the salient spatial or spatio-temporal information, enabling the detection of OOC states even in the presence of complex process patterns. Nevertheless, such data modeling may also lead to practical limitations, e.g., a possibly high computational cost and a large number of model parameters to be fine tuned to achieve desired performances. Moreover, in some cases, modeling complex dynamic patterns impose restricting assumptions on the nature of IC process pattern and/or OOC events, like in Yan et al. (2020).

Another stream of methods was investigated in the literature (Wang and Tsung, 2005, Menafoglio et al., 2018 and various studies reviewed in Megahed et al 2011). The underlying idea consists of transforming high dimensional data (like images and video-image data) into a lower dimensional format (e.g., curves and functions) to make in-line process monitoring compu-

tationally tractable and, at the same time, achieve good anomaly detection performances despite the intrinsic information loss.

Our study belongs to this second stream of research. Due to the big size of video-image data (millions of pixels, tens to thousands of frames per second) it becomes evident that efficient monitoring tools are needed to draw decisions in near real time. More and more frequent industrial problems in digitalized production lines are characterized by big and fast streams of image data but limited data storage capabilities. These problems usually involve also challenging needs for a fast response to possible unstable process states. Aiming to address this kind of problems, the proposed approach grounds on a dimensionality reduction that entails passing from raw input video-image (with possibly high spatial and/or temporal resolution) to a 1D dimensional representation to be used as "signature" of the information enclosed in the frame.

Previous works proposed methods following this path. The seminal study of Wang and Tsung (2005) used the idea of testing with Q-Q plots the conformance of the new incoming images against an IC reference, enabling the adoption of the profile monitoring suite of techniques (Noorossana et al., 2011) to the 1D Q-Q plot pattern. In a different approach, profile monitoring of the empirical probability density function (PDF) of synthetic features extracted from the image was proposed by Menafoglio et al. (2018). Aforementioned methods rely on the assumption that the probability distribution of pixel intensities or extracted features is either known or remains the same in all images acquired under IC conditions. This assumption is not applicable to video image data. Due to the underlying dynamic nature of the process captured in the video, pixel intensities in different frames will have wildly varying distributions that will be rather challenging to characterize using parametric modeling. Thus, non-parametric approaches could be the most promising alternative.

In this study, we suggest the use of the empirical cumulative distribution function (ecdf) of pixel values of each frame, to summarize the process signature in a frame. The ecdf computation is combined with an image pre-processing operation aimed at limiting the analysis of ecdf patterns in consecutive frames to the foreground region only, where relevant process

dynamics occur. Instead of deriving or modeling a reference ecdf during phase I, the proposed approach aims at estimating a benchmark that will demarcate the IC behavior. Thus, we will establish what is the region of ecdf's IC behavior and utilize the partial first order stochastic dominance (PFOSD) properties to test (in-line during phase II) whether the process has moved from the IC to the OOC state (for an extensive bibliographic review on the concept of stochastic dominance refer to Bawa, 1982). Stochastic dominance is a form of stochastic ordering between random variables. More specifically, a random variable X is first order stochastic dominant over another random variable if its cumulative distribution function is lower than the cumulative distribution function of Y over the entire domain. PFOSD is a relaxation of the first order stochastic dominance concept as it entails a dominance over a predetermined subset of the original domain only. In our proposed approach, the random variable of interest is the pixel intensity. Comparing ecdf curves of pixel intensities corresponding to different video frames can be viewed as a PFOSD problem, where the term "partial" refers to the restriction of the range of pixel intensity values to foreground intensities only.

In this framework, we translate the PFOSD into two novel ways of designing non-parametric control charts for video image data. The first, hereafter referred to as "Area Under the ecdf" (AUecdf), exploits as monitoring statistic the area under the ecdf as an empirical index to determine to what extent the ecdf of any newly acquired video frame is dominant with respect to ecdfs observed during phase I. A video frame where the foreground region includes more occurrences of high pixel intensity values can be viewed as stochastic dominant over video frames mainly consisting of low intensity pixels. Thus, the AUecdf approach results into a one-sided control chart aimed at signaling a stochastic dominant pattern with respect to phase I observations, which can be related to an OOC process state.

Since the AUecdf approach implies that only anomalous dominant ecdfs can be signaled as departures from on IC state, a second and more general approach is presented too. It is referred to as "Sandwich ecdf (Secdf)" and it consists of a two-sided control chart suitable to signal anomalous patterns that are either dominant or dominated by the ecdfs observed during

phase I.

It is worth noting that, relying on the ecdf of pixel intensities in each frame and using the AUecdf synthetic statistic, any spatial information about individual pixel locations is not used for process monitoring purposes. Indeed, the field of application of the proposed approach regards industrial problems characterized by the need for both an efficient synthesis of the image or video image information, and a fast and effective response to OOC states. Within this field of research, we show that the proposed approach can outperform benchmark methods, with the further advantage of not requiring any parametric modeling step neither any in-control "template", making the method quite flexible and easily applicable regardless of the underlying (complex) dynamics of the process. Surely, there are other application fields where capturing the spatial and spatio-temporal dynamics of the process may be needed. In these cases, other families of methods should be preferred, like approaches mentioned above or methods that combine dimensionality reduction with spatial weighting schemes (Colosimo and Grasso, 2018).

The two proposed approaches are evaluated and compared in terms of various performance metrics in the presence of both simulated and real data. A robustness analysis with respect to the amount of data available in phase I is presented too. The method proposed in Wang and Tsung (2005), slightly adapted to deal with video image data with an underlying varying signature, is used as a benchmark to highlight the benefits enabled by the novel proposed methods.

1.1 Motivating Case Study

The motivation of this work comes from a real case study in laser powder bed fusion (L-PBF), a metal additive manufacturing process to produce complex shapes by selectively melting a thin layer of metal powder (Gibson et al., 2014). The case study, previously introduced by Grasso et al. (2018) and Grasso and Colosimo (2019), regards the in-situ monitoring of L-PBF of pure zinc via infrared (IR) video imaging. Zinc is a biodegradable material of great industrial

interest for the production of novel and customized biomedical devices. However, due to the low melting and boiling point, the L-PBF of zinc powder is a challenging task, involving the risk for unstable metal vaporization states that could cause not fully dense and defective parts. Figure 1 shows some examples of IR video frames converted into 8-bit grayscale images under IC and OOC conditions. With pixel intensities ranging between 0 (black) and 255 (white), under IC conditions low pixel intensities (dark pixels) refer to background, while high pixel intensities (bright pixels) refer to foreground regions including hot areas of the layer scanned by the laser, hot metal vapor emissions (also known as "plume") and spatters (Grasso and Colosimo, 2019). In this case study, the IC state refers to frames where the existing variation within the frame and from frame to frame can be attributed to the natural result of the L-PBF process at that time, while the OOC state involves frames where there exist exogenous source of variation. More specifically, OOC states can be associated either to excessive material vaporization, like a too large and too hot plume (Figure 1b) or even an exploding plume emission in more severe cases (Figure 1c). The natural process dynamic prevents from defining a reference model, since the laser scans different regions of the build area following a scan path that changes from one layer to another and generates hot by-product emissions whose salient properties continuously change along each scanned track. Because of this, such real case study motivates the development of a new perspective for video image SPC/M and it represents a suitable test bench to evaluate the potential and performance of our proposed approaches.

Despite being motivated by a real case application in AM, the two methods presented in this study are believed to be characterized by a general validity that makes them suitable for other practical SPC/M use cases involving video image data characterized by complex and dynamically changing process patterns. This kind of use cases is becoming more and more frequent in the continuously evolving digitalized manufacturing scenario.

The paper is organized as follows. Section 2 describes the PFOSD methodology. Sections 3 and 4 present the two non-parametric methods for process monitoring, namely the AUecdf and Secdf methods respectively. Section 5 presents a simulation study to demonstrate and com-

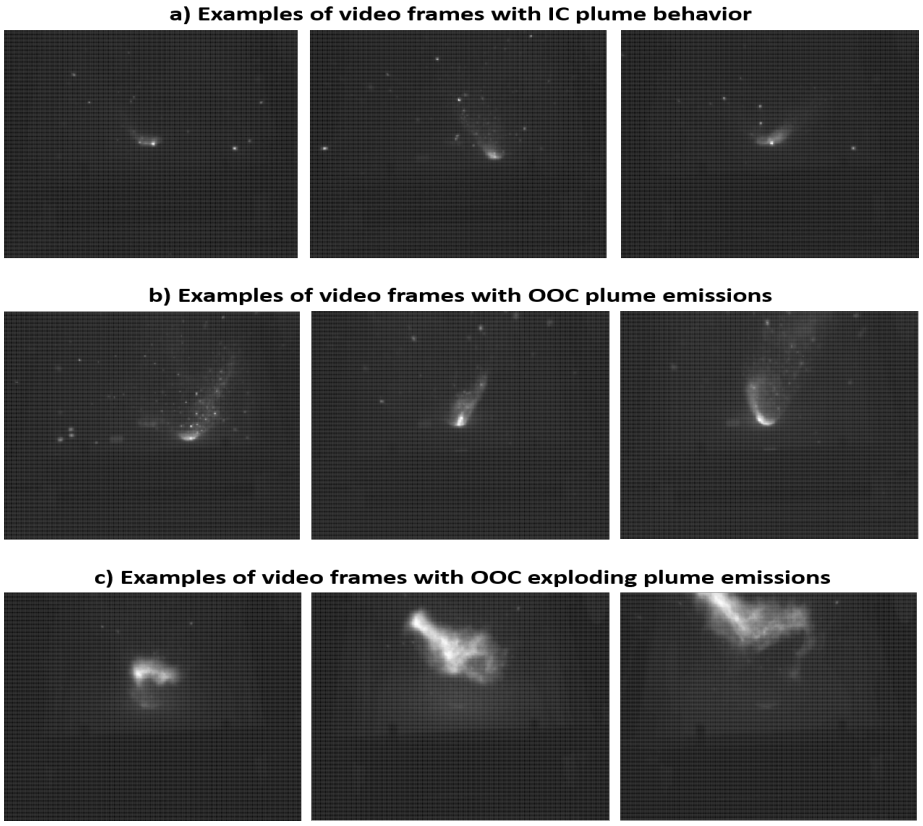

Figure 1: Examples of video frames (converted into 8-bit grayscale images) acquired during the L-PBF process of pure zinc with in-situ / in-line long infrared thermography: a) examples of IC plume emissions, b) and c) examples of OOC plume emissions.

pare the performance of the methods. Section 6 presents the real case study application and Section 7 concludes the paper.

2 (Partial) First Order Stochastic Dominance (PFOSD)

We begin with the basic definition of stochastic dominance on univariate cumulative distribution functions (cdf).

Definition 1 *In the univariate setting, we say that a random variable X with cdf $F_X(\cdot)$ will be*

first order stochastic dominant over the random variable Y with cdf $F_Y(\cdot)$, denoted as $Y \overset{sd}{\leq} X$ if:

$$F_X(t) \leq F_Y(t) \;\; \forall t \in \mathbb{R} \quad \textit{and} \; \exists \, t^* \in \mathbb{R} \quad \textit{such that:} \quad F_X(t^*) < F_Y(t^*) \tag{1}$$

From this point on we will simply refer to the above property as stochastic dominance, implying that we have first order. Alternative names of this property found in literature are stochastic ordering, stochastic greater cdf etc. In case of first order stochastic dominance, the ecdfs are not crossing each other. Various properties are linked to first order stochastic dominance with the most noticeable that:

$$Y \overset{sd}{\leq} X \Rightarrow E[Y] < E[X] \tag{2}$$

or slightly more general, if $h(\cdot)$ is any bounded increasing function we have that:

$$Y \overset{sd}{\leq} X \Rightarrow E[h(Y)] < E[h(X)] \tag{3}$$

The concept of stochastic dominance in practice is a rather strong argument as it requires a pair of cdfs to be ordered and never cross over the entire region of real numbers. A bit less restrictive concept is the partial stochastic dominance, where the first order stochastic dominance is restricted over a predetermined set A. Specifically, we say that $Y \overset{psd_A}{\leq} X$ if:

$$F_X(t) \leq F_Y(t) \;\; \forall t \in A \quad \text{and} \; \exists \, t^* \in A \quad \text{such that:} \quad F_X(t^*) < F_Y(t^*) \tag{4}$$

As a consequence of partial stochastic dominance over a set A we have that:

$$Y \overset{psd_A}{\leq} X \Rightarrow \int_A F_X(t)dt < \int_A F_Y(t)dt \tag{5}$$

i.e. the area under the cdf of X, over the subset A of the support set, will be smaller from the respective area under the cdf of Y. Note that if $A = \mathbb{R}$ then the partial stochastic dominance becomes simply stochastic dominance. In the next section we will carry the concept of (partial) stochastic dominance to empirical cumulative distribution function (ecdf) of images.

2.1 (Partial) Stochastic Dominance in image based ecdfs

For the grayscale video recording that we consider in this work each pixel value can be an integer in the set $\{0, 1, 2, \ldots, 254, 255\}$ where 0/255 refer to absolute black/white. Thus for each frame we can derive the frequency distribution of all possible values reflecting the empirical probability mass function (epmf):

$$\{p_0, p_1, \ldots, p_{254}, p_{255}\}, \quad \text{where} \quad 0 \leq p_i \leq 1,\ i = 0, 1, 2, \ldots, 255 \quad \text{and} \quad \sum_{i=0}^{255} p_i = 1 \tag{6}$$

along with the empirical cumulative distribution function (ecdf):

$$\{P_0, P_1, \ldots, P_{254}, P_{255}\}, \quad \text{where} \quad P_0 = p_0, P_1 = p_0 + p_1, \ldots, P_i = \sum_{j=0}^{i} p_j, \ldots, P_{255} = 1 \tag{7}$$

Given that the support set is a countable finite set, the ecdf will be a step function, where the height of each step occurring at (the support set's) value i, will be equal to p_i, while the total height of the ecdf at i will be P_i. To illustrate the concept of the frame based ecdfs we provide in Figure 2 three scenarios which cover the whole spectrum:

(a) All pixels are black (i.e. take only the value of 0) indicating no action at all. Then:

$$p_0 = 1,\ p_1 = \ldots = p_{255} = 0 \quad \text{and} \quad P_0 = P_1 = \ldots = P_{255} = 1$$

(b) All pixels are white (i.e. take only the value of 255) indicating maximum action. Then:

$$p_0 = p_1 = \ldots = p_{254} = 0,\ \ p_{255} = 1 \quad \text{and} \quad P_0 = P_1 = \ldots = P_{254} = 0,\ \ P_{255} = 1$$

(c) All values $\{0, 1, 2, \ldots, 254, 255\}$ in the support set are equally likely. Then:

$$p_0 = p_1 = \ldots = p_{255} = \frac{1}{256}, \quad \text{and} \quad P_i = \frac{i+1}{256} \quad \text{where } i = 0, 1, 2, \ldots 255$$

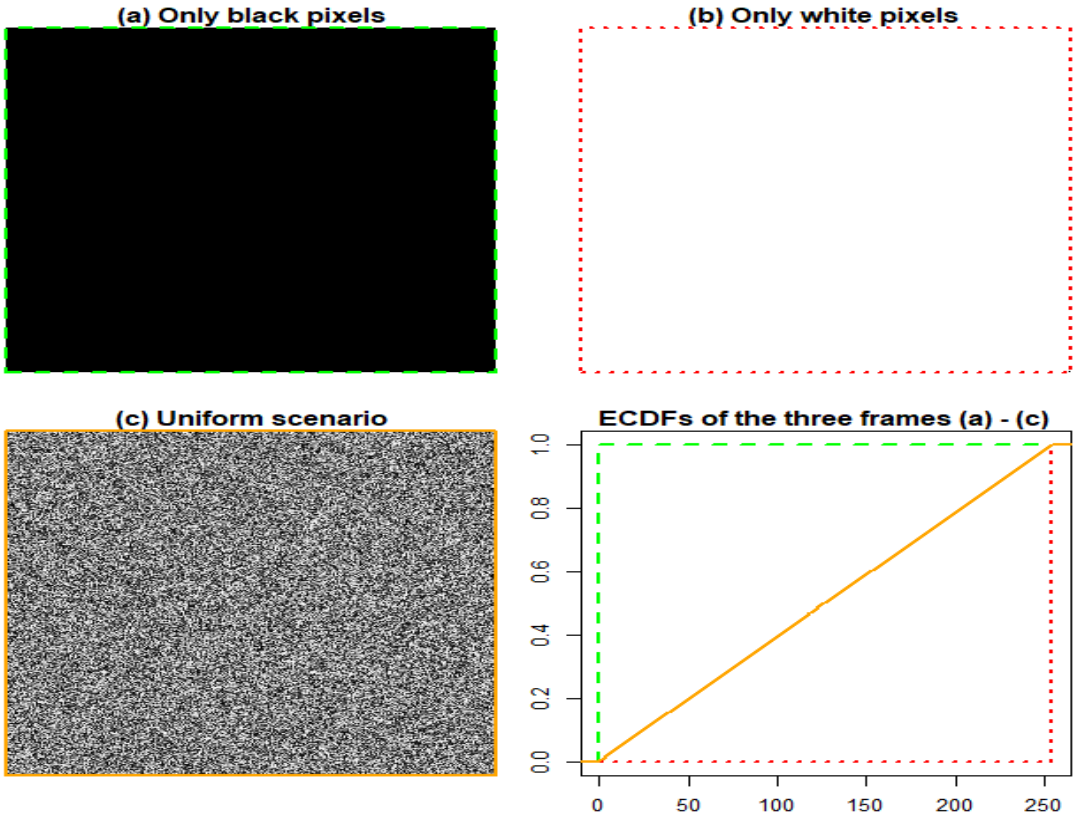

Figure 2: The frames along with the respective ecdfs for three scenarios that span the entire region: (a) only black pixels, (b) only white pixels, (c) all possible pixel values are equally likely and randomly scattered.

For an additive manufacturing application, if the distance of the camera from the region of interest is constant and so is the frame resolution over the working area (i.e. we do not perform zoom in/out) we receive several IC frames that we can use in a phase I exercise to train a monitoring scheme. For each IC frame we can easily derive and plot its ecdf. Figure 3 shows two IC frames along with their respective ecdf, where in one of the two we have more action (yet IC) compared to the other. In this paper, we use the term "action" to the process signature occurring either in IC or OOC conditions. High action means that a large and intense foreground area is observed in the video frame as a consequence of large process by-product emissions. On the contrary, low action, means that few by-product emissions are present, and the video frame mainly consist of uniform and dark background.

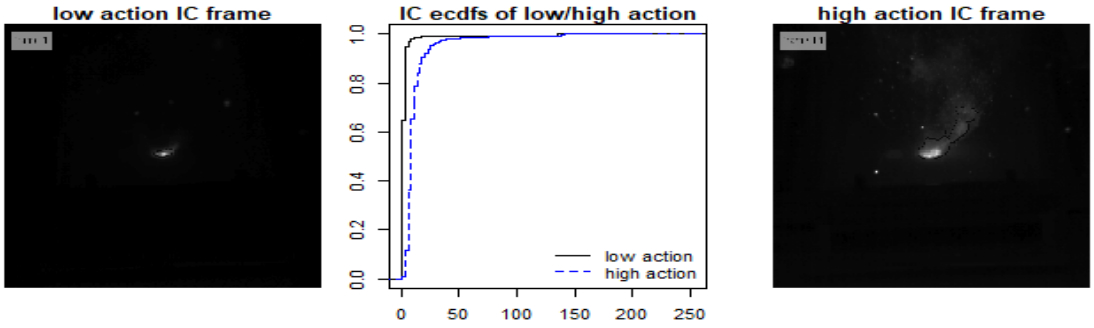

Figure 3: Two IC ecdfs of a low and high IC action frames

In SPC/M, the concept of OOC behavior is typically considered as any scenario that it does not look like what we have during the IC calibration phase. In other words, during phase I we construct some prototype behavior and then during phase II as each new frame becomes available we compare it against the IC prototype, testing of whether it conforms or not. For example Wang and Tsung (2005) looks for discrepancies from the linearity in QQ-plots, Menafoglio et. all (2018) builds the IC type of profile for empirical probability density functions (epdf) and check each new frame for conformance or not etc.

Using ecdfs we will attempt to slightly generalize the concept of testing against an IC prototype frame by moving to the an IC region. The idea of OOC performance in the image based SPC/M that we consider in this study is reflected as enlarged action space (area) compared to what was established during the IC phase I. In other words we expect in OOC situations to have more bright pixels, i.e. an increased portion of the frame with high values compared to the IC video sequence, even at places of the frame that are not close to the area that the laser operates. Generally speaking in the discrete pmf over $\{0, 1, 2, \ldots, 254, 255\}$ as we move from an IC to an OOC frame, chunks of probability mass will travel from the smaller to the bigger values forcing the ecdf to be moved to the right (see Figure 4).

Using standard methods from the literature, if an incoming frame has significantly different (smaller/larger) action region compared to what we established in the IC phase I period, then this frame will not conform to the reference built in phase I and it will alarm. On the contrary, in our approach a frame will result an alarm only if significant probability mass travels

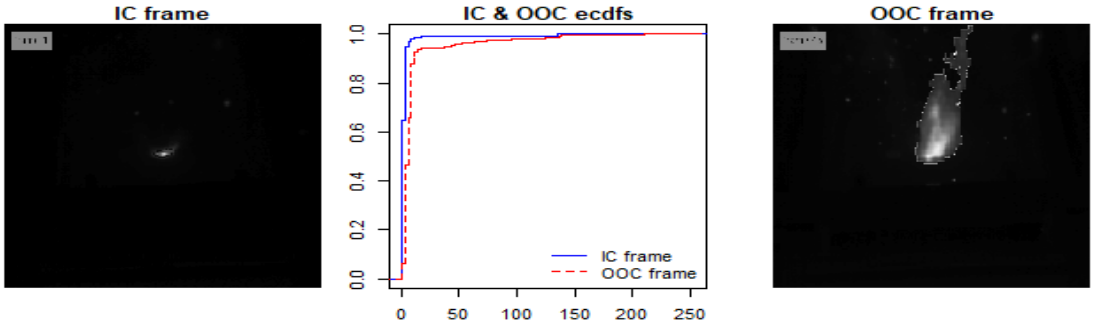

Figure 4: An IC and an OOC frame, along with their respective ecdfs

to the right (i.e. bigger values) driving in the same direction the ecdf. When it travels to the left (i.e. smaller values) then we consider this to conform to the IC region and we do not raise an alarm (compare the ecdf of low IC versus high IC action in Figure 3).

So if we will consider various IC ecdfs, then when a new frame is compared against them, the further to the left/right the ecdf is moving versus the IC ecdfs, the stronger the evidence that the new frame refers to IC/OOC state. Making use of the stochastic dominance concept, the above OOC behavior indicates that OOC ecdfs should (partially) dominate (i.e. be (partially) stochastically greater from) the IC ecdfs. Next, we will utilize the idea of stochastic dominance in ecdfs introducing the summary measure of the area under an ecdf and present two methods that can be used to infer in an online fashion of whether an incoming frame is IC or OOC. Precisely, if we call f_1 and f_2 the ecdfs of two frames, then for the area trapped below them over a predetermined region A, we have by (5):

$$\{f_1 \text{ is PFOSD on A over } f_2\} \Rightarrow \{\text{the area under } f_1 \text{ will be smaller than that under } f_2\}$$

As the converse is not valid, in this manuscript the suggested methods will utilize the contrapositive for identification of the IC frames. Anything that will not comply with this contrapositive rule will indicate OOC performance.

3 Area Under the ecdf (AUecdf) method

It is important to remember that in this study we consider pixel values in a bounded (countable) set, namely $\{0, 1, 2, \ldots, 254, 255\}$, while in other applications, e.g. infrared imaging, we might have each pixel value to refer to temperature, giving rise to an unbounded (uncountable) set. The bounded aspect makes the problem a bit more difficult, as it imposes certain constrains on the ecdfs. For example, all frames will have an ecdf value of 1 at the maximum allowable pixel value 255 (i.e. $F(255) = 1$ for all frames). In this context the idea of stochastic dominance is a very strong requirement that is difficult to be valid when we consider the entire range of the support set (i.e. $\{0, 1, \ldots, 255\}$). In Figure 5 we provide an IC and an OOC frame, where despite their notable difference (even in the ecdf) no stochastic ordering (over the whole support set) can be established, as the ecdfs cross.

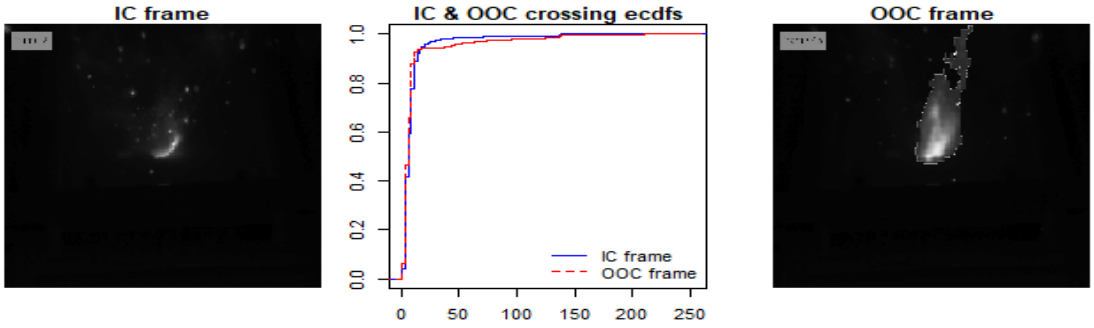

Figure 5: An IC and an OOC frame, with crossed ecdfs

Nevertheless, the upper values of the support set are expected to have inflated probability mass for an OOC frame compared to an IC frame. The situation though at the lower values of the support set is not as clear since these values are quite sensitive to noise, i.e. they are not as helpful in identifying the OOC behavior.

From an image analysis perspective, each frame can be partitioned in the:

- Foreground area, where the action is taking place (relates to high pixel values) and

- Background area, where no significant action is observed, i.e. we can think of it as the quiet region of the frame (relates to the small pixel values on the support set).

Taking into account all the above, one can argue that the foreground region and precisely its extent, i.e. small or large, can reflect the IC or OOC status of a frame respectively. Computer vision provides various algorithms that one could use to obtain the background/foreground separation in each frame. However, the dynamic aspect of the problem under study along with the need to have a low computational cost (to allow near real time inference) makes most of the existing methods prohibitive.

Our proposal will be to utilize partial stochastic dominance of ecdfs over a subset of the support set that relates to the foreground, aiming to be efficient and with low computational cost. Precisely, we will start with an offline calibration phase where:

(A.I.a) Collect N_0 IC phase I frames from the process under study or from historical data of this process. We will initially derive a threshold value called Q_B which will correspond to pixel intensity that separates the background (smaller intensities) from the foreground (higher intensities). The region $S_f = \{Q_{B+1}, Q_{B+2}, \ldots, 254\}$ will be called the foreground support space (the value 255 -upper bound of the support set- was excluded as non-informative, since on this value all ecdfs take the same value of 1).

(A.I.b) For each of the phase I IC frames we estimate the area under ecdf (from now on called AUecdf) over the region S_f, i.e. the foreground support set.

(A.I.c) Use all the AUecdf values estimated in the previous step and derive the lower $\alpha \times 100\%$ point of their distribution as the lower control limit, LL, of the proposed chart. The α value will reflect the desired false alarm rate.

Next we are ready to start phase II, where online testing can be performed on a control chart that will plot AUecdf versus frame number (or time). Specifically, the steps are as follow:

(A.II.a) For each incoming phase II frame i, derive its ecdf and calculate the $AUecdf_i$ over S_f.

(A.II.b) Plot the $AUecdf_i$ versus time and compare it against the lower control limit LL. If $AUecdf_i < LL$ then we draw an alarm.

In what follows we will provide all the details of how the above algorithm can be implemented in practice. Starting with the chart calibration, we will need N_0 representative IC frames of the process under study either from a phase I exercise or from possibly available historical data.

To derive Q_B in step **(A.I.a)**, we will need to know the image's foreground region as percent of the entire frame ($f \times 100\%$). This can be considered as the maximum allowable area of action, when the process is under the IC state. For industrial processes it is possible to evaluate it in advance and is related to the process under study, the distance/zoom of the camera etc. In the case that this percent is not known in advance, it can be estimated from the phase I sequence of the N_0 IC frames. Precisely, for each frame we perform cluster analysis to split the pixels into two groups: background (small) and foreground (large), defining as $f_j \times 100\%$ the percentage of pixel values belonging to the foreground (high values) region of frame $j \in \{1, 2, \ldots, N_0\}$. One of the most widely used methods for such two-level segmentation is the k-means algorithm with $k = 2$, which is also known to be computationally efficient. Next, for each of the N_0 IC frames derive the pixels value Q_B^j so that:

$$G_j(Q_{B-1}^j) < 1 - f_j \leq G_j(Q_B^j) \tag{8}$$

where $G_j(\cdot)$ is the ecdf of all pixel values of frame j. In other words for each frame j we identify Q_B^j, which corresponds to the pixel intensity above which we have the $f_j \times 100\%$ percent of the highest pixel intensities that refer to foreground. If the $f \times 100\%$ was available in advance then we do not need to perform clustering and in relationship (8), we replace f_j by f for all frames. Then we estimate the overall Q^B as the mean of the N_0 intensities $\left\{Q_B^1, \ldots, Q_B^j, \ldots, Q_B^{N_0}\right\}$, which is rounded to the closest integer with greater than or equal intensity (i.e. ceiling) and we finalize the foreground support set as: $S_f = \{Q_{B+1}, Q_{B+2}, \ldots, 254\}$.

In step **(A.I.b)**, for each of the N_0 IC frames we derive the AUecdf over the subset S_f. As we have a discrete random variable then for every frame $j \in \{1, 2, \ldots, N_0\}$ we will have:

$$AUecdf_j = \sum_{x \in S_f} F_j(x) = F_j(Q_{B+1}) + F_j(Q_{B+2}) + \ldots + F_j(253) + F_j(254) \tag{9}$$

where, $F_j(\cdot)$ is the ecdf corresponding to frame $j \in \{1, 2, \ldots, N_0\}$.

Next in step **(A.I.c)** we use all estimated $AUecdf_j,\ j = 1, 2, \ldots, N_0$ to get their distribution and derive the lower control limit LL as the lower α quantile, where α refers to the predetermined false alarm rate that we wish to have. The limit LL demarcates the IC region, where the smaller the AUecdf (over S_f) is, the more the evidence that the current frame is OOC as the observed probabilities for the high intensity pixels are elevated indicating an extended region of foreground action compared to what we expect from the phase I calibration. So as opposed to establish in phase I, a prototype ecdf curve against which future frame ecdf's will be examined (a philosophy typically followed from other methods in the literature), we define a lower limit below which we have evidence that the frame examined will partially dominate the behavior observed in phase I. An AUecdf value, does not correspond to a single ecdf, as various ecdfs can have the same AUecdf (i.e. it is not one-to-one) and so the limit LL does not really correspond to a specific (prototype) ecdf established in phase I but instead puts the limit on the distribution of the AUecdf values observed in phase I. The Area under the ecdf forms a synthetic descriptor, capable to diagnose scenarios of partial stochastic dominance (over the foreground intensity values) that are likely to occur in OOC conditions. It does not require to have some prototype to compare against (as it happens in similar studies) and allows direct use to processes, where the underlying spatio/temporal dynamics of the process are difficult or computationally expensive to model. However, for processes where the OOC states of interest have either a local effect and/or affect the spatio-temporal history of pixel intensities rather than their ecdf in each image, other relevant methods should be used instead.

The suggested control chart will plot the AUecdf value versus time with the horizontal line at LL splitting the IC/OOC regions as the area above/below LL. Putting the N_0 frames

of the calibration phase on the control chart only $\alpha \times 100\%$ of the frames will be below LL. In phase II we operate in online fashion, where as a new frame arrives, we estimate its AUecdf over S_f and plot the result in the control chart, raising an alarm if we are below the LL line. As it is typically suggested in SPC/M when we get an alarm the user needs to stop the process examine the root cause of the alarm, possibly take some corrective action and restart the whole mechanism. Algorithm 1 provides in detail all the steps to obtain the Area Under ecdf control chart for a process monitored with grayscale camera.

4 The Sandwich ecdfs method

The motivation in the AUecdf method was to derive a lower limit (LL), based on the phase I input, that reflects on the maximum allowable size of the foreground region. So in phase II, if for a frame we have an AUecdf value (over S_f) smaller than LL that indicates an ecdf that will partially stochastically dominate the IC ecdfs (of phase I), having a foreground region that is too "large" (i.e. we have an enlarged plume or explosion or spatters etc.). Thus in the AUecdf method, our interest is for one-sided tests only (i.e. against enlarged foreground). What happens though if a frame in phase II has a foreground region that is too "small" (shrank)? For instance, the laser has a problem and stops working, diminishing the foreground region. In that case, the AUecdf will consider this frame as IC (as the phase I ecdfs will tend to partially stochastically dominate it). To identify such frames as OOC we will need to have a two-sided scheme that will "sandwich" the phase I IC ecdfs and indicate as OOC the frames that will tend to have either too "large" (i.e. ecdfs will partially stochastically dominate the ecdfs of phase I) or too "small" (i.e. ecdfs will be partially stochastically dominated by the ecdfs of phase I) foreground region.

Our proposal will be to create an IC region that will bound ("sandwich") stochastically the phase I IC ecdfs and judge in phase II each incoming ecdf against this region. Specifically, a partial stochastic dominance based score will indicate in a control chart of whether the process is IC or we have an enlarged or shrank foreground region, compared to the phase I standards that

Algorithm 1 Area Under the ecdf (AUecdf)

Phase I (offline)
Obtain N_0 representative IC frames (from phase I or historical data) ▷ *initial input*
Define the desired false alarm rate: α
for $(j = 1, 2, \ldots N_0)$ **do** ▷ *loop over phase I IC frames*
    if (image foreground region ratio over all pixels is known and constant to$f$) **then**
        $f_j \leftarrow f$
    else
        Use k-means clustering to split the frame pixels in $k = 2$ groups
        The small/large clustered values, constitutes the Background/Foreground region
        Define as f_j the ratio of the foreground pixels over all pixels in the frame j
    end if
    Obtain Q_B^j so that relationship (8) is satisfied
end for
Define $Q_B \leftarrow ceiling\left\{mean\left(Q_B^1, \ldots, Q_B^j, \ldots, Q_B^{N_0}\right)\right\}$
Define the foreground support set as: $S_f = \{Q_{B+1}, Q_{B+2}, \ldots, 254\}$
for $(j = 1, 2, \ldots N_0)$ **do** ▷ *loop over phase I IC frames*
    Obtain $AUecdf_j$ using (9)
end for
Define $LL \leftarrow \alpha$ empirical quantile of $\{AUecdf_1, \ldots, AUecdf_j, \ldots, AUecdf_{N_0}\}$
Phase II (online)
Create a 2D control chart of AUecdf values versus frame number.
Add on the chart the horizontal control limit LL.
$i \leftarrow 1$
for (frame i in phase II) **do** ▷ *loop over phase II frames*
    Obtain the ecdf of frame i using (7)
    Obtain $AUecdf_i$ using (9) and plot it on the control chart
    if $(AUecdf_i < LL)$ **then**
        Raise an alarm: the current frame is in the OOC region
    end if
    $i \leftarrow i + 1$
end for

we will denote as OOC state 1 or 2 respectively. We begin with an off-line calibration scheme where we:

(S.I.a) Collect N_0 IC phase I frames from the process under study or from historical data of this process and obtain the ecdf of each of the N_0 frames.

(S.I.b) Obtain the lower and upper stochastic limits that will sandwich the $(1-\alpha)\times 100\%$ ecdfs of phase I at each pixel intensity value. The α value aims to robustify the limits against possible outlying frames in phase I. These limits split the 2d space of $\{0, 1, 2, \ldots, 254\}\times[0, 1]$ where the ecdfs are plotted, in three zones:

- IC: within stochastic limits
- OOC1: below the lower stochastic limit indicating that we have frames that stochastically dominate the phase I frames (i.e. foreground region is too large).
- OOC2: above the upper stochastic limit indicating that we have frames stochastically dominated by the phase I frames (i.e. foreground region is too small).

(S.I.c) We use the above three zones to partition each phase I IC frame j into three segments, based on the overlap of its ecdf with the three zones: IC, OOC1 and OOC2 respectively. Next we weight each of the three segments of the ecdf accordingly and we derive an overall score SC_j.

(S.I.d) Use all the SC_j scores ($j = 1, 2, \ldots, N_0$) estimated in the previous step and derive the lower $\alpha^\star/2$ and the upper $1-\alpha^\star/2$ point of their distribution as the lower (L) and upper (U) limits respectively, of the proposed control chart. The choice of $\alpha^\star$ value will reflect the desired false alarm rate.

Next, phase II can be started allowing online testing on a control chart that will plot the stochastic dominance based score versus frame number (or time). The steps are as follow:

(S.II.a) For each incoming phase II frame i derive its ecdf and calculate the score SC_i.

(S.II.b) Plot SC_i versus its order and compare it against the lower/upper control limits. If:

- $L \leq SC_i \leq U$ the frame is in par with the IC phase I frames
- $SC_i < L$ raise an OOC1 alarm (expanded foreground compared to phase I).
- $SC_i > U$ raise an OOC2 alarm (shrank foreground compared to phase I).

Next, we will explain and motivate all the details of the above algorithm. Initially, we will need N_0 representative IC frames of the process under study either from a phase I exercise or from possibly available historical data. At **(S.I.a)** we will derive the ecdf of each IC frame j of Phase I using (7), i.e. $\left\{P_0^{(j)}, P_1^{(j)}, \ldots, P_k^{(j)}, \ldots, P_{254}^{(j)}, 1\right\}, j = 1, 2, \ldots, N_0$.

In step **(S.I.b)** for each specific intensity value $k \in \{0, 1, \ldots, 254\}$ we bound the distribution of all phase I ecdfs at k using the lower $(\alpha/2)$ and upper $(1 - \alpha/2)$ empirical quantile. Precisely we derive:

$$\begin{aligned} L_k^\alpha &= \frac{\alpha}{2} \text{ empirical quantile of } \left\{P_k^{(1)}, P_k^{(2)}, \ldots, P_k^{(j)}, \ldots, P_k^{(N_0)}\right\} \\ U_k^\alpha &= \left(1 - \frac{\alpha}{2}\right) \text{ empirical quantile of } \left\{P_k^{(1)}, P_k^{(2)}, \ldots, P_k^{(j)}, \ldots, P_k^{(N_0)}\right\} \end{aligned} \tag{10}$$

for each $k \in \{0, 1, \ldots, 254\}$. The α value relates to the stochastic limit derivation and it aims to provide some robustness against the presence of outlying phase I frames. Then we define as lower (L^α) or upper (U^α) stochastic limits of phase I ecdfs:

$$L^\alpha = \{L_0^\alpha, L_1^\alpha, \ldots, L_k^\alpha, \ldots, L_{254}^\alpha\} \quad \text{and} \quad U^\alpha = \{U_0^\alpha, U_1^\alpha, \ldots, U_k^\alpha, \ldots, U_{254}^\alpha\} \tag{11}$$

The stochastic limits will "sandwich" the $(1-\alpha)\times 100\%$ of the observed ecdf values for each intensity value in the support set $\{0, 1, \ldots, k, \ldots, 254\}$ (intensity 255 was excluded as non-informative since all ecdfs get the same value, i.e. 1). Therefore, the limits L^α and U^α will partition the 2d region: $\{0, 1, \ldots, 254\} \times [0, 1]$ in three non-overlapping zones: IC, OOC1 and OOC2 , as described in **(S.I.b)**

In next step, **(S.I.c)**, for each phase I frame $j, (j = 1, 2, \ldots, N_0)$ we derive an overall

score SC_j, relying on the overlap of its ecdf $F_j(\cdot)$ with the three 2d-zones. Precisely, for each pixel intensity $k, (k = 0, 1, 2, \ldots, 254)$, we define:

$$SC_j^{(k)} = \left\{ \begin{array}{cl} -1 & \text{if } (k, F_j(k)) \text{ lies in the OOC1 zone} \\ 0 & \text{if } (k, F_j(k)) \text{ lies in the IC zone} \\ 1 & \text{if } (k, F_j(k)) \text{ lies in the OOC2 zone} \end{array} \right\} \tag{12}$$

and then for the whole frame j we obtain the average score:

$$SC_j = \frac{1}{255} \left[\sum_{k=0}^{254} SC_j^{(k)} \right] \tag{13}$$

The frame score SC_j will be a number in $[-1, +1]$. In the last phase I calibration step, **(S.I.d)**, we derive the lower (L) and upper (U) limits of the distribution of all phase I scores using the lower $(\alpha^\star/2)$ and upper $(1 - \alpha^\star/2)$ empirical quantile respectively, i.e.:

$$\begin{aligned} L &= \frac{\alpha^\star}{2} \text{ empirical quantile of } \{SC_1, SC_2, \ldots, SC_j, \ldots, SC_{N_0}\} \\ U &= \left(1 - \frac{\alpha^\star}{2}\right) \text{ empirical quantile of } \{SC_1, SC_2, \ldots, SC_j, \ldots, SC_{N_0}\} \end{aligned} \tag{14}$$

The control limits will define a region $[L, U] \subset [-1, +1]$, which will indicate conformance with the IC standards. Scores that plot outside the $[L, U]$ region, indicate OOC behavior and specifically values that are smaller (larger) compared to $L(U)$, will provide evidence that we have a frame with enlarged (shrank) foreground region compared to the IC phase I frames. Thus, just like we did in the AUecdf methodology, we avoid to derive some IC prototype but instead we define regions where the OOC frames will tend to have their ecdfs lying, depending on whether they dominate or get dominated by the phase I IC ecdfs.

The proposed control chart will plot the score (SC_j) value versus time along with two control limits at L, U, which will mark the IC region, while values bellow (above) $L(U)$ will denote OOC1 (OOC2) scenarios. Initially, we will plot the N_0 phase I calibration frames on the control chart, where only $\alpha^\star \times 100\%$ of the frames will plot outside $[L, U]$. In phase II we move

to online inference, where as a new frame i arrives, we calculate its score SC_i and plot it in the control chart, raising an OOC1 (OOC2) type of alarm if we are below (above) the $L(U)$ control limit. As we mentioned in AUecdf method, when we get an alarm we need to stop the process examine the root cause of the alarm, take some corrective action (if available) and restart the whole mechanism. Algorithm 2 provides in detail all the steps to obtain the "Sandwich ecdf" control chart for a process monitored with grayscale camera.

Sandwich modification:
The Sandwich ecdf method works with the ecdfs over the entire region $\{0, 1, 2, \ldots, 254\}$ of the parameter space. Following the foreground/background separation defined in the AUecdf methodology, we could apply the Sandwich ecdf method only at the foreground support set $S_f = \{Q_{B+1}, Q_{B+2}, \ldots, 254\}$ to utilize further the partial stochastic dominance properties. The motivation behind the use of the foreground region S_f, instead of the whole range [0,254] in both methods lies in the fact that the PFOSD is more evident in the upper tail of the ecdf in OOC situations as opposed to the lower values, where ecdfs tend to cross more often independently of whether we are in the IC or OOC state (see also Figure 5).

5 Simulation study

5.1 Simulation settings

The aim of the simulation study discussed in this section was to evaluate and compare the performances of the two proposed approaches in the presence of artificial but realistic out-of-control video image patterns with controlled severity.

IC and OOC realizations of video frames were generated by processing a real sequence of video frames acquired during the production of zinc samples via L-PBF. The starting real dataset is the one gathered in our real case study (all details are discussed in Section 6) and

Algorithm 2 Sandwich the ecdf (Secdf)

Phase I (offline)
Obtain N_0 representative IC frames (from phase I or historical data) ▷ *initial input*
Define the critical value α, needed in determining the stochastic limits
Define the desired false alarm rate $\alpha^\star$, for the Sandwich control chart
for $(j = 1, 2, \ldots N_0)$ **do** ▷ *loop over phase I IC frames*
    Obtain the ecdf of frame j: $\left\{P_0^{(j)}, P_1^{(j)}, \ldots, P_k^{(j)}, \ldots, P_{254}^{(j)}, 1\right\}$ using (7)
end for
for $(k = 0, 1, \ldots 254)$ **do** ▷ *loop over intensity values*
    Obtain $L_k^\alpha \leftarrow \alpha/2$ empirical quantile of $\left\{P_k^{(1)}, P_k^{(2)}, \ldots, P_k^{(j)}, \ldots, P_k^{(N_0)}\right\}$
    Obtain $U_k^\alpha \leftarrow (1 - \alpha/2)$ empirical quantile of $\left\{P_k^{(1)}, P_k^{(2)}, \ldots, P_k^{(j)}, \ldots, P_k^{(N_0)}\right\}$
end for
Define $L^\alpha \leftarrow \{L_0^\alpha, L_1^\alpha, \ldots, L_k^\alpha, \ldots, L_{254}^\alpha\}$
Define $U^\alpha \leftarrow \{U_0^\alpha, U_1^\alpha, \ldots, U_k^\alpha, \ldots, U_{254}^\alpha\}$
for $(j = 1, 2, \ldots N_0)$ **do** ▷ *loop over phase I IC frames*
    for $(k = 0, 1, \ldots 254)$ **do** ▷ *loop over intensity values*
        Obtain $SC_j^{(k)}$ using (12)
    end for
    Obtain SC_j using (13)
end for
Obtain $L \leftarrow \alpha^\star/2$ empirical quantile of $\{SC_1, SC_2, \ldots, SC_j, \ldots, SC_{N_0}\}$
Obtain $U \leftarrow (1 - \alpha^\star/2)$ empirical quantile of $\{SC_1, SC_2, \ldots, SC_j, \ldots, SC_{N_0}\}$
Phase II (online)
Create a 2D control chart of SC_j score values versus frame number.
Add on the control chart the horizontal control limits L and U.
$i \leftarrow 1$
for (frame i in phase II) **do** ▷ *loop over phase II frames*
    Obtain the ecdf of frame i
    Obtain its score SC_i using (13) and plot it on the control chart
    if $(SC_i < L)$ **then**
        Raise an alarm: the current frame is in the OOC1 region (enlarged foreground)
    end if
    if $(SC_i > U)$ **then**
        Raise an alarm: the current frame is in the OOC2 region (shrank foreground)
    end if
    $i \leftarrow i + 1$
end for

the following image processing steps were applied. First, a pool of about 300 real video frames was extracted from the original database. They were labelled as IC because the manufactured samples showed high density and no evident defect. Then, an image thresholding operation based on the Otsu's method (Otsu, 1979) was used to segment each frame into a background region and a foreground region, where the latter includes the plume emission and any other bright area. This segmentation could have been achieved by the Q_B threshold used in the suggested methodology, but instead we preferred to apply Otsu's method and other basic image preprocessing techniques, so that the simulated data generation mechanism has nothing in common to the data analysis methods. A second step was applied to isolate the plume from all other foreground regions, by setting a threshold on the size of each connected component and the location of its centroid. The result of this operation was checked by a human expert to validate the proper identification of the plume region in each frame.

The following step was aimed at generating a larger number of IC realizations of video frames by randomly rescaling and changing the aspect ratio of the connected component labelled as "plume". Two scaling factors δ_x and δ_y were applied along the x and y directions of the image, respectively, such that $\delta_x = 1 + 0.1k_x$ and $\delta_y = 1 + 0.1k_y$ with k_x and k_y independently drawn from a uniform distribution $U(0, 5)$. A total number of 2,200 unique video frames were generated by applying random combinations of k_x and k_y. They were used as IC video frames to design the control charts (first 200 frames) and test the IC performance (last 2,000 frames).

Four different OOC scenarios were then simulated, where the x and y directions of the plume area were rescaled by $\delta_x + \Delta_x$ and $\delta_y + \Delta_y$, such that the terms Δ_x and Δ_y were used to insert OOC shifts of different severity.

- OOC scenario 1 refers to a linearly increasing trend of the plume size, which can be representative of a heat accumulation in the part as the process goes on, leading to larger and larger plume emissions. OOC scenario 1 was simulated by setting both Δ_x and Δ_y linearly increasing from 1 (first video frame) to Δ_{max} (last video frame), where four different severity levels were considered with Δ_{max} ranging between 1 and 4.

- OOC scenario 2 is representative of a non-sustained shift lasting for only three consecutive video frames. In this case, the rescaling factors were δ_x and δ_y, in frames with no shift and $\delta_x + \Delta_x$ and $\delta_y + \Delta_y$ in frames with the OOC shift, and same severity levels of scenario 1 for Δ_x and Δ_y were used.

- OOC scenario 3 presents of a sustained shift, where in all frames the plume was rescaled by $\delta_x + \Delta_x$ and $\delta_y + \Delta_y$ with the same severity levels of previous scenarios for Δ_x and Δ_y.

- OOC scenario 4, eventually, is representative of sudden (unsustained) shifts that become more and more frequent as the severity increases. This kind of OOC behavior is representative of the real anomalies observed in our real case study. In this scenario, whenever a sudden shift occurred, the plume was rescaled by $\delta_x + \Delta_{max}$ and $\delta_y + \Delta_{max}$, and the frequency of shifts increased from 10% to 80% with a random ordering of OOC shifts.

In each simulation run, 465 OOC video frames were generated for each scenario and each severity level (4 scenarios $\times$ 4 severities = 16 OOC cases). The OOC video frames were always preceded by 2000 IC frames for the proper estimation of all performance metrics, i.e.:

$$Sensitivity = \frac{TP}{TP + FN}, \qquad Specificity = \frac{TN}{TN + FP} \qquad \text{and}$$

$$Accuracy = \frac{TP + TN}{TP + TN + FP + FN} \tag{15}$$

where TP is the number of true positives, FP is the number of false positives, TN is the number of true negatives and FN is the number of false negatives.

The PFOSD for both the proposed approaches used only a subset of pixel intensities resulting from the preliminary segmentation into foreground and background via k-means clustering, with $k = 2$. According to this operation, pixel with intensity in the range $\{0, 1, \ldots, 31\}$ were labelled as background pixels, belonging to cold (dark) areas, not affected by the process and its by-products. Pixels with intensity in the range $\{32, 33, \ldots, 255\}$ were instead labelled as foreground pixels, and defined the region of the ecdfs where the stochastic dominance phe-

nomenon was examined. In both suggested methods the autocorrelation of the summary statistic used in the monitoring was examined for possible time dependence and it found to be quite low. This is somewhat expected as the area under ecdf is a summary measure of the deconstructed frame (via its ecdf) and thus there is no need to involve some time dependence in either AUecdf or Secdf monitoring schemes.

The two methods were also compared against the seminal method proposed by Wang and Tsung (2005), although a slight adaptation was needed to transfer it to video image data, rather than to sequences of images of the same object. In Wang and Tsung (2005) each monitored image was translated into a 1-D profile format through the computation of a Q-Q plot, using the normal distribution as in-control reference. In video image data capturing dynamic processes, it is not possible to identify a reference distribution for the pixel intensity values, and hence the benchmark Q-Q plot-based approach was here implemented by using, as a reference for the Q-Q plot definition, the quantiles of pixel intensities obtained by averaging all phase I video frames. For each video frame, the Q-Q plot curve was fitted through a least square regression model of order 1 and two control charts were designed: a Hotelling's T^2 control chart on the two parameters of the regression model and a univariate control chart on the mean square error of the model residuals. This competitor approach is referred to as "QQplot" in what follows.

The control charts for the two proposed methods were designed with a type I error $\alpha = 0.01$. The competitor approach based on the Q-Q plot modeling and monitoring was design with a familywise type I error $\alpha = 0.01$ using Bonferroni's correction.

5.2 Simulation study results

The performances of all compared methods are summarized in Table 1, in terms of sensitivity, specificity and accuracy metrics. Table 1 shows that the two proposed approaches have similar performance metrics. The Secdf method is the one characterized by the highest sensitivity in all simulated OOC scenarios, but its accuracy is slightly lower than the one of the AUecdf method

in most cases, which is connected to a slightly lower specificity in identifying true negatives. The high sensitivity highlights the capability of signaling actual OOC shifts. The benchmark approach based on the Q-Q plot modeling and monitoring is less effective than the proposed methods, resulting in a much lower sensitivity, i.e. lower capability of detecting actual OOC patterns. Indeed, the Q-Q plot-based approach is designed for monitoring process data that are identically distributed and the distribution is known. In the presence of video image data like the ones considered in this study, the distribution of the pixel intensity values is not known, and it may change from frame to frame. Under these premises, extracting a reference distribution from phase I data (e.g., the distribution of pixel intensities obtained by averaging out all phase I video frames) leads to a wild variability of Q-Q plot patterns under IC conditions as shown in Figure 6, including curves that can be approximated by order 1 models but also Q-Q plot curves with very different pattern. Such variability, partially masks actual OOC shifts unless their severity is sufficiently high.

		Sensitivity [%]			**Specificity** [%]			**Accuracy** [%]		
	Severity	AUedcf	Secdf	QQplot	AUedcf	Secdf	QQplot	AUedcf	Secdf	QQplot
Scenario 1	1	26.67	**28.60**	0.22	98.75	97.20	**99.30**	**85.15**	84.26	80.61
	2	40.00	**44.73**	1.08	98.75	97.20	**99.30**	**87.67**	87.30	80.77
	3	50.11	**53.33**	5.16	98.75	97.20	**99.30**	**89.57**	88.92	81.54
	4	58.28	**60.22**	15.05	98.75	97.20	**99.30**	**91.12**	90.22	83.41
Scenario 2	1	53.33	**60.00**	0.00	98.77	97.17	**99.30**	**98.22**	96.71	98.09
	2	76.67	**83.33**	6.67	98.81	97.25	**99.18**	**98.54**	97.08	98.05
	3	77.78	**81.48**	22.22	98.77	97.17	**99.22**	**98.54**	97.00	98.38
	4	80.00	**83.33**	46.67	98.69	97.21	**99.30**	98.46	97.04	**98.66**
Scenario 3	1	48.17	**55.27**	0.00	98.75	97.20	**99.30**	89.21	**89.29**	80.57
	2	71.40	**76.56**	7.74	98.75	97.20	**99.30**	**93.59**	93.31	82.03
	3	85.59	**86.67**	24.95	98.75	97.20	**99.30**	**96.27**	95.21	85.27
	4	92.69	**92.90**	55.70	98.75	97.20	**99.30**	**97.61**	96.39	91.08
Scenario 4	1	**91.84**	**91.84**	61.22	98.76	97.06	**99.30**	**98.62**	96.96	98.54
	2	**94.90**	**94.90**	46.94	98.86	97.42	**99.24**	**98.70**	97.32	97.16
	3	92.06	**92.59**	56.61	98.86	97.32	**99.25**	**98.34**	96.96	95.98
	4	91.33	**92.14**	53.66	98.71	97.14	**99.33**	**97.61**	96.32	92.49

Table 1: Performance metrics (in percentage) for AUecdf, Secdf and QQplot methods (boldface entries indicate the best performance across the three competitors)

Figures 7 and 8 present the AUecdf and the Secdf control charts respectively, in all

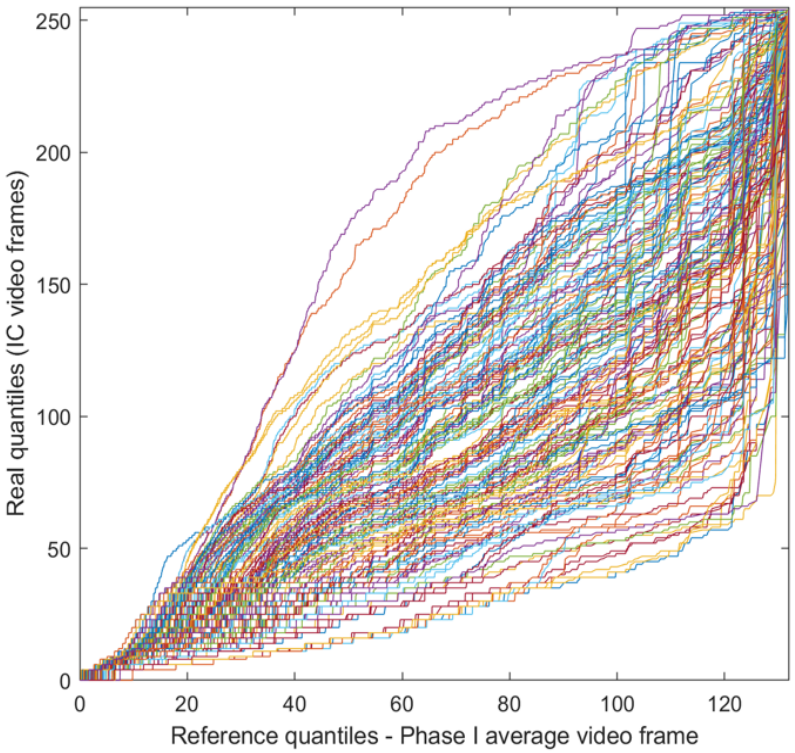

Figure 6: Q-Q plot curves corresponding to 200 IC video frames, where reference quantiles refer to pixel intensities obtained by averaging out all phase I video frames.

simulated OOC scenarios for all different severity levels (the ecdfs plots for both IC and OOC data can be found in the Appendix). Each panel of Figures 7 and 8 shows the phase II control chart in one specific OOC scenario for one specific severity level, over all 465 simulated frames. Figures 7 and 8 indicate that both the number of true positives and the entity of signaled shifts grow as the OOC severity grows. Figure 8 also shows that, although all simulated OOC conditions entailed a violation of the lower control limit, some violations of the upper control limit are present as well in OOC scenario 1, 2 and 4. Such violations are labelled as false positives in this specific case. They correspond to frames where the foreground pixel intensity was first order stochastically dominated by the intensities observed in phase I, i.e., video frames whose foreground pixel exhibited a significantly darker pattern with respect to the ones used for control chart design. Although being labelled as false positives, generally speaking they represent actual anomalies with respect to patterns observed in phase I. Thus, the capability of signaling

such anomalies as well, makes the Secdf approach of greater general validity than the AUecdf approach.

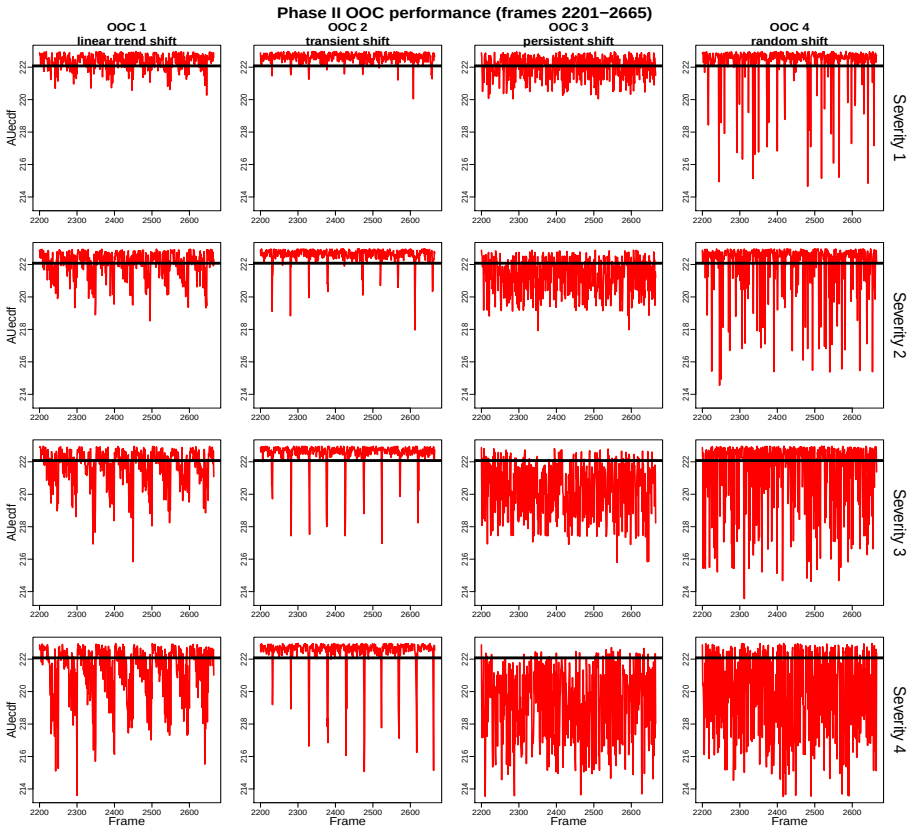

Figure 7: Phase II AUecdf control charts in different OOC scenarios (columns) and different severity levels (rows); the solid black line represents the lower control limit of the control chart.

5.3 Robustness analysis

The results reported in subsection 5.2 referred to a phase I consisting of $L = 200$ video frames. However, for in-line monitoring applications, particular interest is devoted to the robustness of the adopted method with respect to the amount of data used for control chart design. As a matter of fact, the smaller is L, the sooner the control chart can be used to monitor the ongoing process. To this aim, in this Section we compare the performances of the AUecdf and Secdf methods by varying the number of frames used in phase I, namely the L parameter. This analysis was based

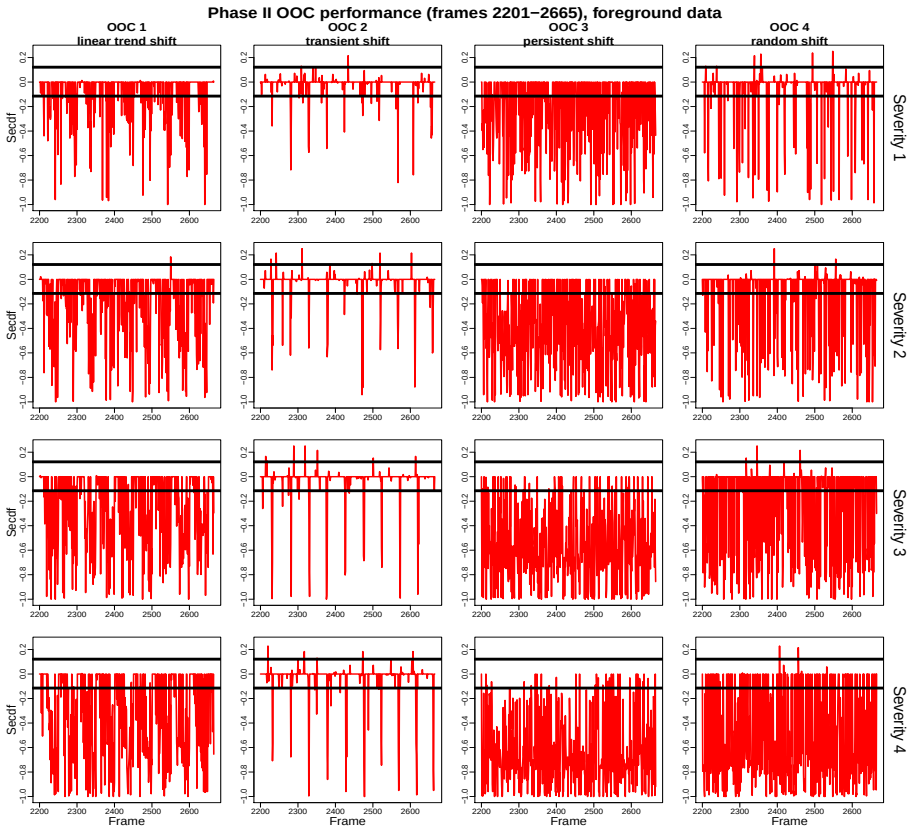

Figure 8: Phase II Secdf control charts in different OOC scenarios (columns) and different severity levels (rows); the solid black lines represent the lower and upper control limits of the control chart.

on the sensitivity metric only, since it is the one suitable to determine the capability of signaling an actual OOC state.

Figure 9 shows the sensitivity of the AUecdf and Secdf control charts as a function of the severity level for different OOC scenarios and for different sizes, L, of the dataset used in phase I. Figure 9 shows that by varying L in the range 10 to 200, a very limited change of the AUecdf control chart sensitivity is observed. This indicates that, even in the presence of a very short design phase, the control chart keeps its ability of detecting OOC shifts. The Secdf method, on the contrary, is much less robust than the AUecdf method. Indeed, its sensitivity considerably drops to low values as L decreases. This is due to the two-sided Secdf monitoring approach that, in case of few phase I observation, may be too conservative causing a high type

II error.

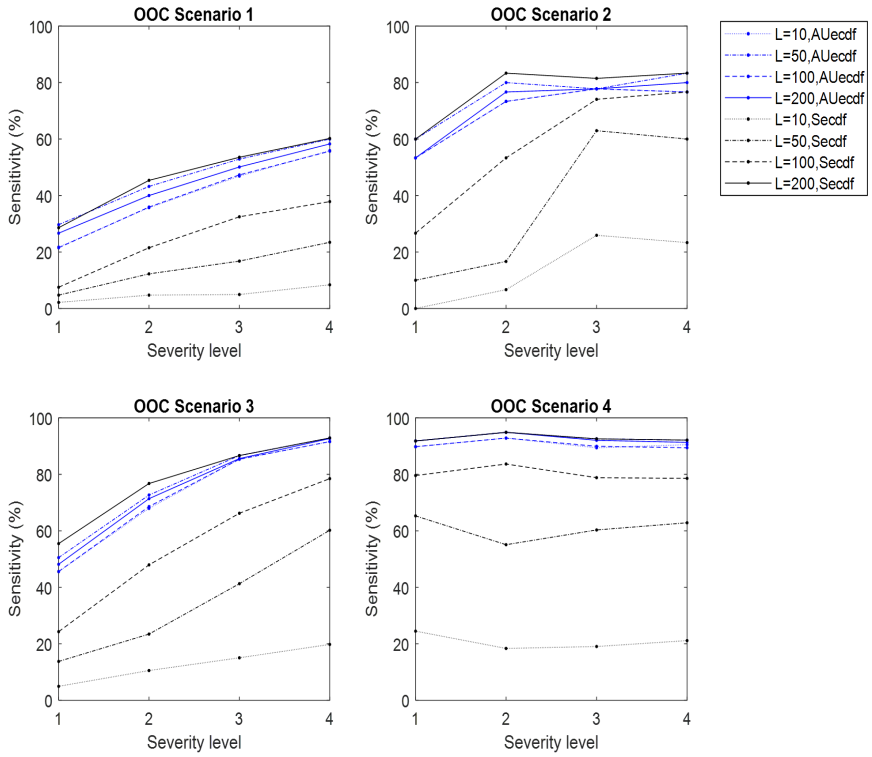

Figure 9: Sensitivity of the AUecdf and Secdf control charts for different OOC scenarios (as a function of the severity level) for different sizes, L, of the dataset used in phase I for control chart design.

The performance analysis carried out in subsections 5.2 and 5.3 allows drawing the following conclusions, which could also be used as guidelines to choose the most appropriate approach:

- The AUecdf method is effective and robust even in the presence of a very limited phase I dataset; being based on a one-sided control charting scheme, it represents a suitable approach when expected OOC conditions involve pixel intensity patterns that stochastic dominate the ones under IC conditions.
- The Secdf method is a more general approach, being based on a two-sided control charting scheme, enabling the detection of anomalies corresponding to pixel intensity patterns

that are either stochastic dominating the patterns observed during phase I or stochastic dominated by them. However, by construction, the Secdf is less robust than the AUecdf method to limited availability of phase I data.

- Both the methods are more effective than the benchmark competitor based on profile monitoring of pixel intensities' Q-Q plots. The outperformance of the AUecdf and Secdf methods are due to the fact that they do not need any estimation of an IC reference distribution. The PFOSD approach represents a suitable and non-parametric alternative whenever the process is characterized by natural dynamics that prevent the definition of a reference distributional model.

6 Real Data Application

6.1 Experimental settings

The real case application that motivated the proposed methodology involves the in-situ monitoring of the L-PBF process during the production of pure zinc samples. Pure zinc belongs to the family of biodegradable materials, hence is suitable for the production of biomedical implants like cardiovascular stents that dissolute inside the human body once fulfilled their duty. L-PBF of pure zinc is particularly interesting thanks to the design complexity and high customization enabled by the additive process, but zinc is highly prone to vaporization under laser irradiance, which makes the production of defect-free parts a challenging task. Because of the intense and hot metal vaporization generated as by-product of the process, in-situ and in-line thermal video imaging could provide relevant information about the process stability. The real case study presented in this paper was previously introduced by Grasso et al. (2018) and Grasso and Colosimo (2019). A prototype L-PBF system equipped with a fiber laser source with 1 kW maximum power was used to produce cubic samples of size $5 \times 5 \times 5$ mm exploiting different sets of process parameters: three sets of process parameters that led to dense parts (density in the range 96.2 -

98.7% measured with the Archimedes's method) and two different sets of parameters that led to OOC process states and severely defective parts. Both IC and OOC sets of process parameters are summarized in Table 2. During the same process other samples were produced, but they are not included into this analysis as they were outside the field of view of the thermal camera.

Process state	**Process parameter set**	**Sample name**	**Laser power** $P(W)$	**Scan speed** $v(mm/s)$	**Hatch distance** $h_d(\mu m)$
IC	1	S1, S8	110	475	160
	2	S4	195	679	160
	3	S7	195	475	160
OOC	4	S3	195	475	78
	5	S5	195	270	160

Table 2: IC and OOC L-PBF process parameters (more details can be found in Grasso and Colosimo, 2019)

In-situ thermal videos were acquired by means of a FLIR SC3000 camera with a long infrared (IR) spectral range of $8-9\mu m$. Thermal videos were acquired with a sampling frequency $f_s = 50Hz$ and a frame size of 311×421 pixels. Figure 10 shows the in-situ sensing setup and the manufactured samples.

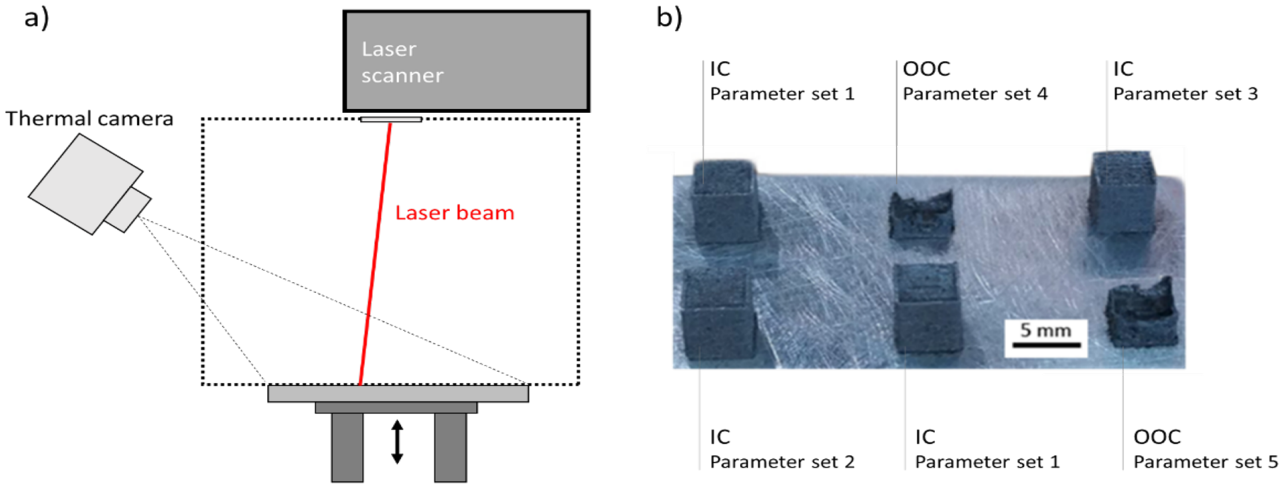

Figure 10: a) Thermal camera setup for in-situ / in-line L-PBF process monitoring; b) samples produced by varying the process parameters leading to either IC or OOC process states.

Thermal camera calibration for absolute temperature estimation is known to be a challenging task in L-PBF, since the material undergoes phase changes from powder to molten pool

to solidified material with production of vaporized material as well (Colosimo and Grasso, 2020). Such phase changes involve quick spatio-temporal variations of the material emissivity whose accurate estimate is needed to convert the raw radiance measurement into absolute temperature values. However, for in-situ monitoring purposes, the knowledge of the absolute temperature is not strictly necessary, since the key issue is the variation of the thermal signature from one frame to another, regardless of the measurement unit. Because of this, in the real case study no IR camera calibration was applied. Moreover, the raw IR video frames were automatically compressed as 8-bit grayscale images, with pixel intensity ranging from 0 (black/cold) to 254 (white/hot). This makes the proposed approach applicable to video image in the visible range as well, without modifications.

The dataset consists of 14 IR videos gathered in 11 non-consecutive layers. During each video, all six samples are sequentially scanned by the laser, and portions of videos corresponding to each single sample where manually extracted to evaluate the performance of the proposed approaches for different process states. In the real case study, the segmentation into foreground and background via k-means clustering, led to the estimation of the ecdfs only for pixels with intensity in the range $\{36, 37, \ldots, 254\}$. The proposed methods were implemented by using the video frames acquired during the production of the first monitored layer as phase I dataset, whereas video frames acquired in all following monitored layers were used as phase II data.

6.2 Real case study results

Figure 11 shows the ecdf of foreground pixel intensities of all samples in different layers. Phase I ecdfs (green curves) are superimposed to the Phase II ecdf curves in all following layers to highlight the increasing entity of the OOC shifts (red dotted curves) as the process goes on. Such increasing entity of OOC deviations is due to a gradually inflating heat accumulation in the part as more and more layers are produced, which results into a more and more intense material vaporization (large and hot plume emissions) when unproper process parameters are applied. Under IC conditions, instead, the process's plume emissions remain stable during the

production of each layer and from one layer to another. In the last monitored layer (i.e., layer 11), the three most severe OOC shifts correspond to three frames where an exploding plume emission took place (the one shown in Figure 1c). Such large or even exploding plume emission is responsible for an excessive material evaporation and attenuation of the laser beam, with a consequent unstable variation of the energy input to the material. Since a larger and hotter plume emission results into a large number of high intensity pixels, the associated ecdf is first order stochastic dominant over the ecdf of IC video frames where a smaller and more stable plume is present.

Figures 12 and 13 show the AUecdf and Secdf control charts in all monitored layers. Since different samples were sequentially scanned by the laser in each layer, vertical bands of different colors were used to distinguish the time windows during which each sample was produced. More specifically, vertical pink bands indicate the time windows during which OOC samples (S3 and S5) were scanned by the laser. Vertical gray bands indicate the time windows during which samples outside the monitored field of view of the camera were produced (they are not included into the present analysis). Eventually, white bands indicate the time windows during which IC samples were produced.

Table 3 summarizes the performances of the AUecdf and Secdf methods in terms of percentage of video frames signalled as alarms in different layers and for different samples. In this case, labelling each alarm as a true or false positive is difficult, since the plume emissions exhibit sudden variations from one frame to another and the OOC state is characterized by intermittent rather than permanent shifts. Because of this, the performance metrics used in the simulation study are not directly applicable. The percentage of signaled alarms was used, instead. The results summarized in Table 3 show that the AUecdf and Secdf methods signal several alarms during the production of the OOC samples S3 and S5, but the main difference between the two methods relies in their performances for IC samples. Indeed, the alarm rate of the AUecdf method under IC conditions is consistent with the target type I error used for control chart design. On the contrary, the Secdf method signals many alarms under IC conditions. A

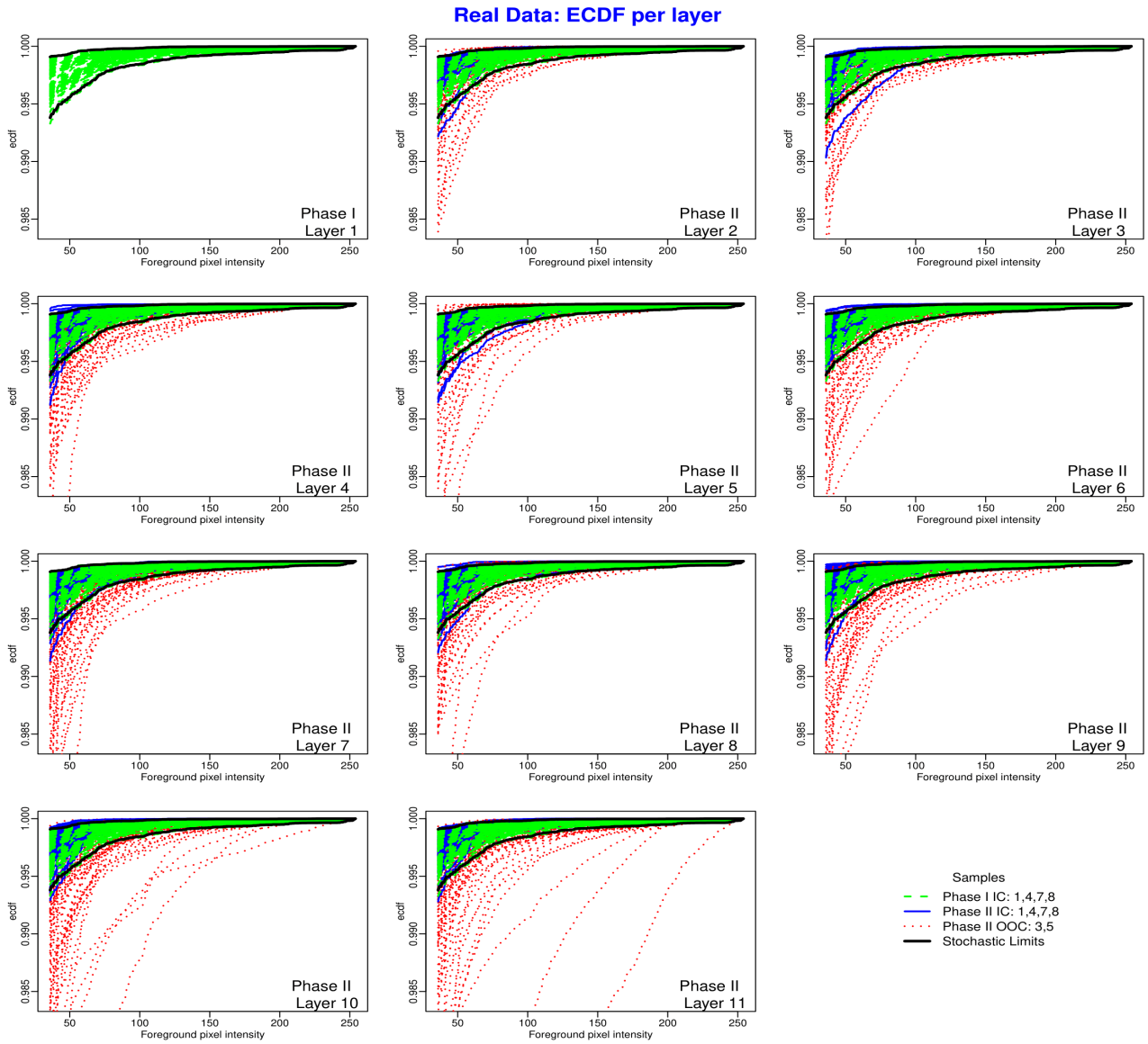

Figure 11: Ecdf of foreground pixel intensities of all samples in different layers. Phase I ecdfs (green curves) are superimposed to the Phase II ecdf curves in all following layers. Blue solid lines correspond to samples (1, 4, 7, 8) produced under IC conditions, whereas red dotted lines correspond to samples (3, 5) produced under OOC conditions. The boldface black lines refer to the stochastic limits used by the Secdf method.

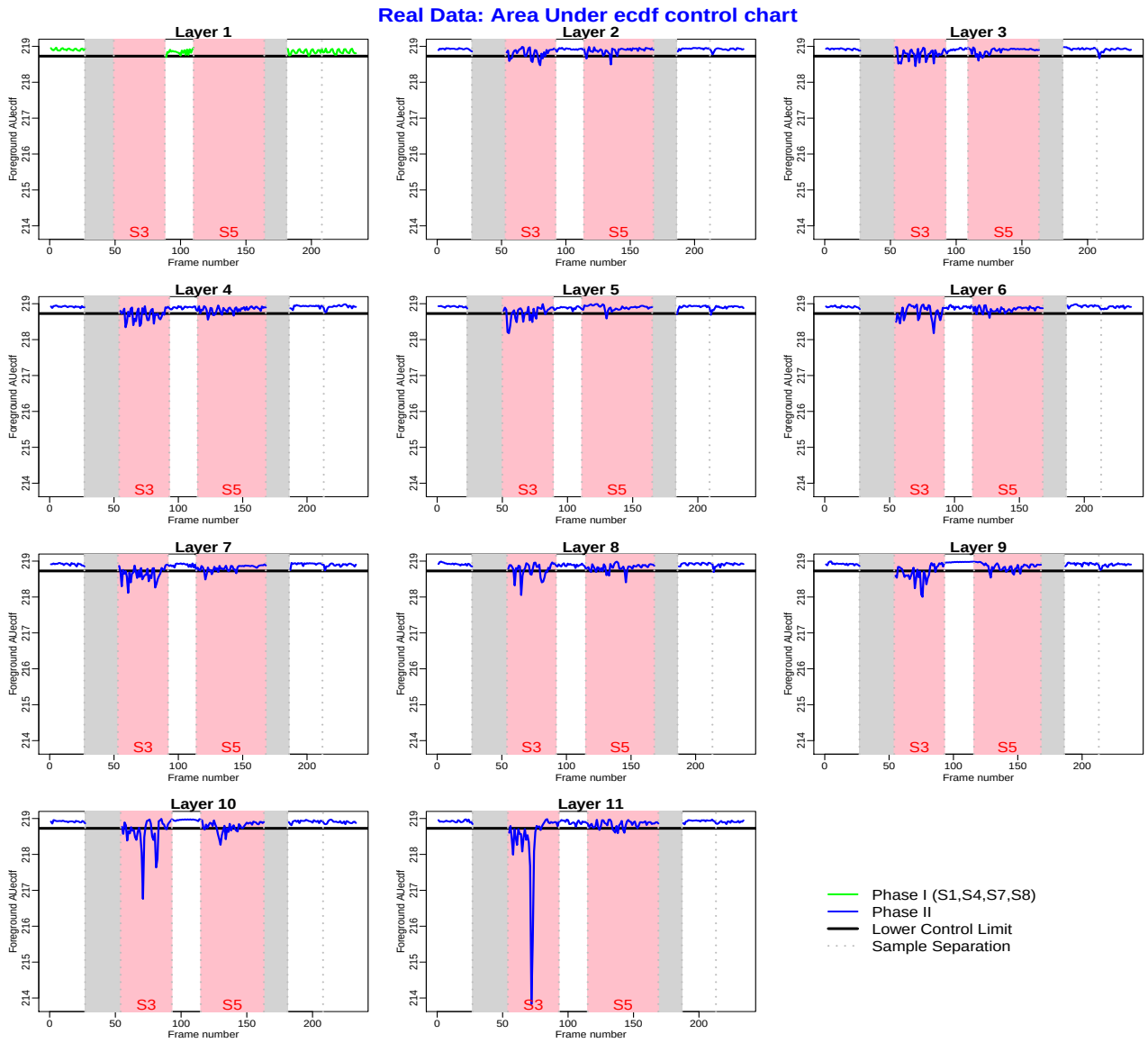

Figure 12: AUecdf control charts in all monitored layers (Phase I corresponds to the first layer, Phase II corresponds to all other layers); vertical pink bands indicate the time windows during which OOC samples (S3 and S5) were scanned by the laser; vertical gray bands indicate the time windows during which samples outside the monitored field of view were produced; white bands indicate the time windows during which IC samples were produced.

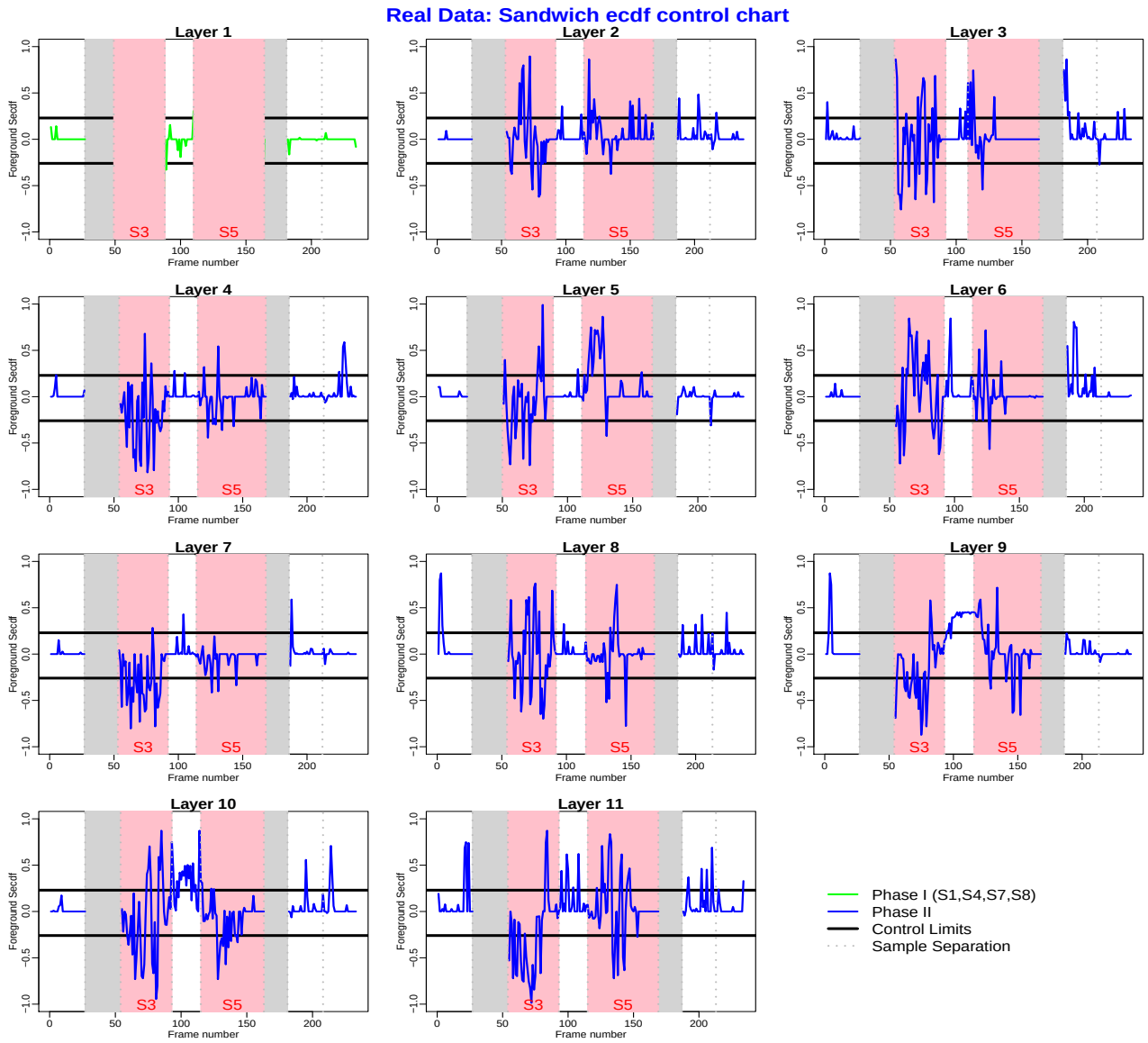

Figure 13: Secdf control charts in all monitored layers (Phase I corresponds to the first layer, Phase II corresponds to all other layers); vertical pink bands indicate the time windows during which OOC samples (S3 and S5) were scanned by the laser; vertical gray bands indicate the time windows during which samples outside the monitored field of view were produced; white bands indicate the time windows during which IC samples were produced.

better insight about this behavior is provided by Table 4, which separately shows the percentage of crossing upper and lower control limits in the Secdf control chart, and Figure 13.

	AUecdf			**Secdf**		
	IC samples	**OOC samples**		**IC samples**	**OOC samples**	
Layer	**S1, S4, S7, S8**	**S3**	**S5**	**S1, S4, S7, S8**	**S3**	**S5**
1	1.96	–	–	1.96	–	–
2	0.00	23.08	5.56	5.94	30.77	18.52
3	1.04	28.21	7.41	13.54	51.28	9.26
4	0.00	51.28	11.32	6.93	41.03	13.20
5	2.06	35.90	1.85	2.06	33.34	27.78
6	0.00	42.11	7.41	8.08	63.16	9.26
7	0.00	64.10	11.11	1.98	56.41	5.56
8	0.99	28.95	15.09	7.92	47.36	13.21
9	0.00	56.41	11.54	22.55	46.16	25.00
10	0.00	51.28	25.00	18.81	51.29	27.08
11	0.00	53.85	12.96	14.58	46.16	33.33

Table 3: Percentage of video frames signalled as alarms by the AUecdf and Secdf methods for IC and OOC process conditions.

	Crossing lower limit			**Crossing of upper limit**		
	IC samples	**OOC samples**		**IC samples**	**OOC samples**	
Layer	**S1, S4, S7, S8**	**S3**	**S5**	**S1, S4, S7, S8**	**S3**	**S5**
1	0.98	17.95	20.37	0.98	2.56	0.00
2	0.00	17.95	1.85	5.94	12.82	16.67
3	1.04	25.64	1.85	12.50	25.64	7.41
4	0.00	35.90	9.43	6.93	5.13	3.77
5	1.03	23.08	1.85	1.03	10.26	25.93
6	0.00	26.32	1.85	8.08	36.84	7.41
7	0.00	53.85	5.56	1.98	2.56	0.00
8	0.00	23.68	5.66	7.92	23.68	7.55
9	0.00	41.03	9.62	22.55	5.13	15.38
10	0.00	28.21	20.83	18.81	23.08	6.25
11	0.00	41.03	12.96	14.58	5.13	20.37

Table 4: Percentage of violations of lower and upper control limits in the Secdf method.

Table 4 and Figure 13 show that the high alarm rate of the Secdf method under IC conditions is caused by violations of the upper control limit, i.e., video frames whose ecdfs are first order stochastically dominated by ecdfs observed during phase I. A few examples of video

frames belonging to this category are shown in Figure 14. In Figure 14, we observe that these frames are characterized by almost no plume emission and they are signaled as alarms since such low plume emission was not observed during the control chart design phase. In the real case study presented here, a one-sided monitoring approach fits well the nature of the OOC signature of plume emissions, which leads to a first order stochastic dominance over patterns deemed IC. However, the Secdf entails a two-sided monitoring scheme that has a more general validity for applications where anomalies of interest could be associated not only to first stochastic dominant patterns but also patterns that are first order stochastically dominated by IC ecdfs.

Figure 14: Example of video frames that led to a violation of the upper control limit in the Secdf control chart.

7 Concluding Remarks

The way in which statistical quality modelling and monitoring methods are designed and implemented in the manufacturing industry shall adapt to a continuously evolving digitalized framework. The sources of information are more and more in the form of real-time sensor signals, image and video image data. High value-added applications move from mass production to highly customized products, but also from simple shapes to complex and innovative geometries. In this scenario, quality engineers shall face novel challenges and they need novel statistical methods. The present study proposed a statistical process monitoring approach that aims to tackle some of these challenges. First, the information enclosed in video image data, related to complex process signature, is translated into a synthetic format through the estimation of the ecdf of pixel inten-

sities. Then, the partial stochastic dominance methodology is used to determine whether newly acquired video frames are IC or OOC. Being a non-parametric approach, it allows dealing with any natural and, at the same time, dynamically changing process behavior. Both the simulation analysis and the application to a real case study in additive manufacturing showed that this method could outperform other techniques that, despite relying on a similar data synthesis step, fail in dealing with naturally changing process signature. The proposed approach was presented in form of two control charting schemes, a one-sided (AUecdf), suitable to detect anomalies and OOC states, formed by an inflation of the process intensity and variability, and a more general one (Secdf), based on a two-sided control chart. The AUecdf resulted to be also quite robust to the number of training IC observations, which is a nice-to-have property in small-lot or even one-of-a-kind frameworks, where little to no historical data are available, and few initial observations during the present process shall be used for control chart design. The Secdf is less robust but characterized by a wider validity, as is allows detecting OOC realizations associated not only to first stochastic dominant patterns but also patterns that are first order stochastic dominated by IC ecdfs. Thus, the choice of the most appropriate method is application-dependent, and, more precisely, it depends on the nature of OOC events of interest. Future research directions may be envisaged to tune the proposed methodology. In particular, rather than relying on a phase I/phase II separation, so called "self-starting" methods can be used to combine training and monitoring since the very beginning of the process, coping with the lack of historical data and aiming to anticipate the detection of possible anomalies. Furthermore, apart from the area under the ecdf concept proposed in this manuscript, other features like the foreground area, could be involved in the modeling leading to multivariate monitoring. The proposed methods can also be extended and tested in the presence of different video image data formats (e.g., calibrated temperature measurements, color video images or multispectral images), not necessarily limited to manufacturing applications.

8 Supplementary material

The data set used in the real case study in Section 6 is available to download in Figshare at the url: https://doi.org/10.6084/m9.figshare.14829033

9 Acknowledgments

We would like to thank the editor and the two anonymous referees, whose valuable comments and suggestions improved significantly the manuscript. This work was supported by the project SIADD: Soluzioni Innovative per la qualitá e la sostenibilitá dei processi di ADDitive manufacturing (Novel solutions for quality and sustainability of AM processes)- MIUR PON MIUR "Ricerca e Innovazione".

References

[1] V. S. Bawa, (1982), "Stochastic Dominance: A Research Bibliography", *Management Science*, 28(6), pp. 698-712.

[2] Bui, A. T., and Apley, D. W., (2018), "A monitoring and diagnostic approach for stochastic textured surfaces", *Technometrics*, 60(1), pp. 1-13.

[3] Colosimo, B. M., Huang, Q., Dasgupta, T., and Tsung, F. (2018), "Opportunities and challenges of quality engineering for additive manufacturing", *Journal of Quality Technology*, 50(3), pp. 233-252.

[4] Colosimo, B.M., Grasso, M., (2018), "Spatially weighted PCA for monitoring video image data with application to additive manufacturing", *Journal of Quality Technology*, 50(4), pp. 391-417.

[5] Colosimo, B.M., Grasso, M., (2020), "On-machine measurement, monitoring and control", chapter 13 in "Precision Metal Additive Manufacturing", edited by R. Leach and S. Carmignato, CRC Press, Taylor & Francis Group.

[6] Deming, W. E. (1986), Out of Crisis, The MIT Press.

[7] Everton, S. K., Hirsch, M., Stravroulakis, P., Leach, R. K., and Clare, A. T., (2016), "Review of in-situ process monitoring and in-situ metrology for metal additive manufacturing", *Materials and Design*, 95, pp. 431-445.

[8] Gibson, I., Rosen, D. W., and Stucker, B., (2014), Additive manufacturing technologies (Vol. 17), New York: Springer.

[9] Grasso, M., Colosimo, B.M., (2019), "A Statistical Learning Method for Image-based Monitoring of the Plume Signature in Laser Powder Bed Fusion", *Robotics and Computer-Integrated Manufacturing*, 57, pp. 103-115.

[10] Grasso, M., Demir, A.G., Previtali, B., Colosimo, B.M., (2018), "In-situ Monitoring of Selective Laser Melting of Zinc Powder via Infrared Imaging of the Process Plume", *Robotics and Computer-Integrated Manufacturing*, 49, pp. 229-239.

[11] He, Z., Zuo, L., Zhang, M. and Megahed, F. M.,(2016), "An image-based multivariate generalized likelihood ratio control chart for detecting and diagnosing multiple faults in manufactured products", *International Journal of Production Research*, 54(6), pp. 1771-1784.

[12] Kan, C., Chen, R., and Yang, H. (2017), "Image-guided quality control of biomanufacturing process", *3rd CIRP Conference on BioManufacturing*, 65, pp. 168-174.

[13] Koosha, M., Noorossana, R., and Megahed F., (2017), "Statistical process monitoring via image data using wavelets", *Quality Reliability Engineering, International*, 33, pp. 2059-2073.

[14] Megahed, F. M., Woodall, W.H., and Camelio, J.A., (2011), "A Review and Perspective on Control Charting with Image Data" *Journal of Quality Technology*, 43(2), pp. 83-98.

[15] Megahed, F.M. Wells, L.J., Camelio, J.A., and Woodall, W. H., (2012), "A Spatiotemporal Method for the Monitoring of Image Data", *Quality Reliability Engineering, International*, 28, pp. 967-980.

[16] Menafoglio, A., Grasso, M., Secchi, P. and Colosimo B.M., (2018), "Profile Monitoring of Probability Density Functions via Simplicial Functional PCA with application to Image Data", *Technometrics*, 60(4), pp. 497-510.

[17] Noorossana, R., Saghaei, A., and Amiri, A., (2011), Statistical analysis of profile monitoring (Vol. 865), John Wiley & Sons.

[18] Otsu, N., (1979), "A threshold selection method from gray-level histograms", *IEEE transactions on systems, man, and cybernetics*, 9(1), pp. 62-66.

[19] Prats-Montalbán, J.M., and Ferrer, A., (2014), "Statistical process control based on Multivariate Image Analysis: A new proposal for monitoring and defect detection" *Computers and Chemical Engineering*, 71, pp. 501-511.

[20] Qiu, P., and Sun, J., (2007), "Local smoothing image segmentation for spotted microarray images", *Journal of the American Statistical Association*, 102(480) pp. 1129-1144.

[21] Wang, K., and Tsung, F., (2005), "Using profile monitoring techniques for a data-rich environment with huge sample size", *Quality and Reliability Engineering International*, 21(7), 677-688.

[22] Yan, H., Grasso, M., Paynabar, K., and Colosimo, B.M., (2020), "Penalized Spatio-temporal Regression for Anomaly Detection in Video-Imaging Data with Application to Hot-spot Detection in Laser Powder Bed Fusion", in press in IISE Transactions (available on ArXiv).

[23] Yan, H., Paynabar, K., and Shi, J., (2015), "Image-Based Process Monitoring Using Low-Rank Tensor Decomposition", *IEEE Transactions on Automation Science and Engineering*, 12(1), pp. 216-227.

Appendix

Figures 15 to 18 show the edcf of pixel intensities in phase I and phase II video frames included into the simulation study presented in Section 5, for different OOC scenarios and different severity levels.

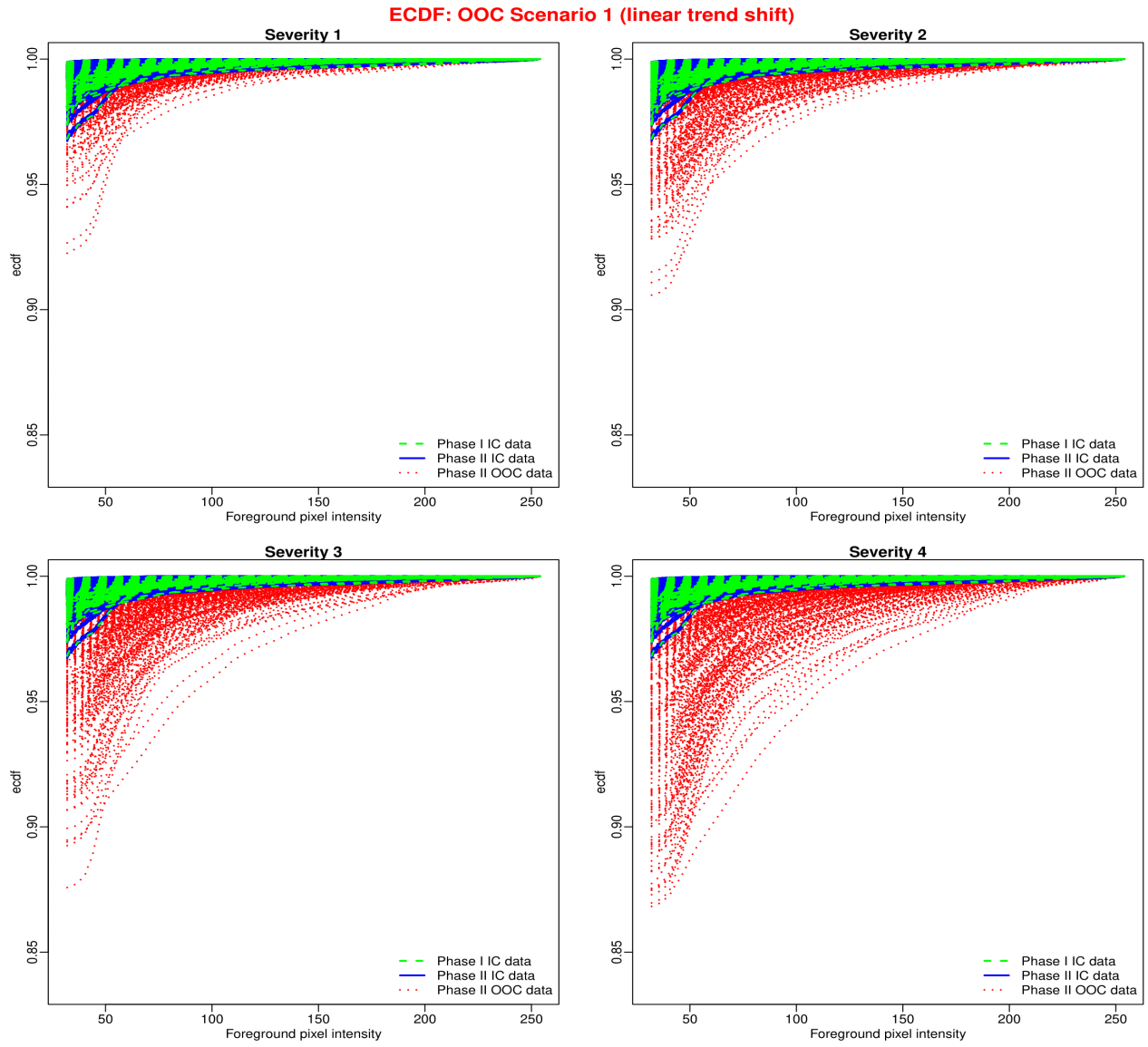

Figure 15: Ecdfs of phase I and phase II video frames in OOC scenario 1 included in the simulated study (different panels refer to different severity levels).

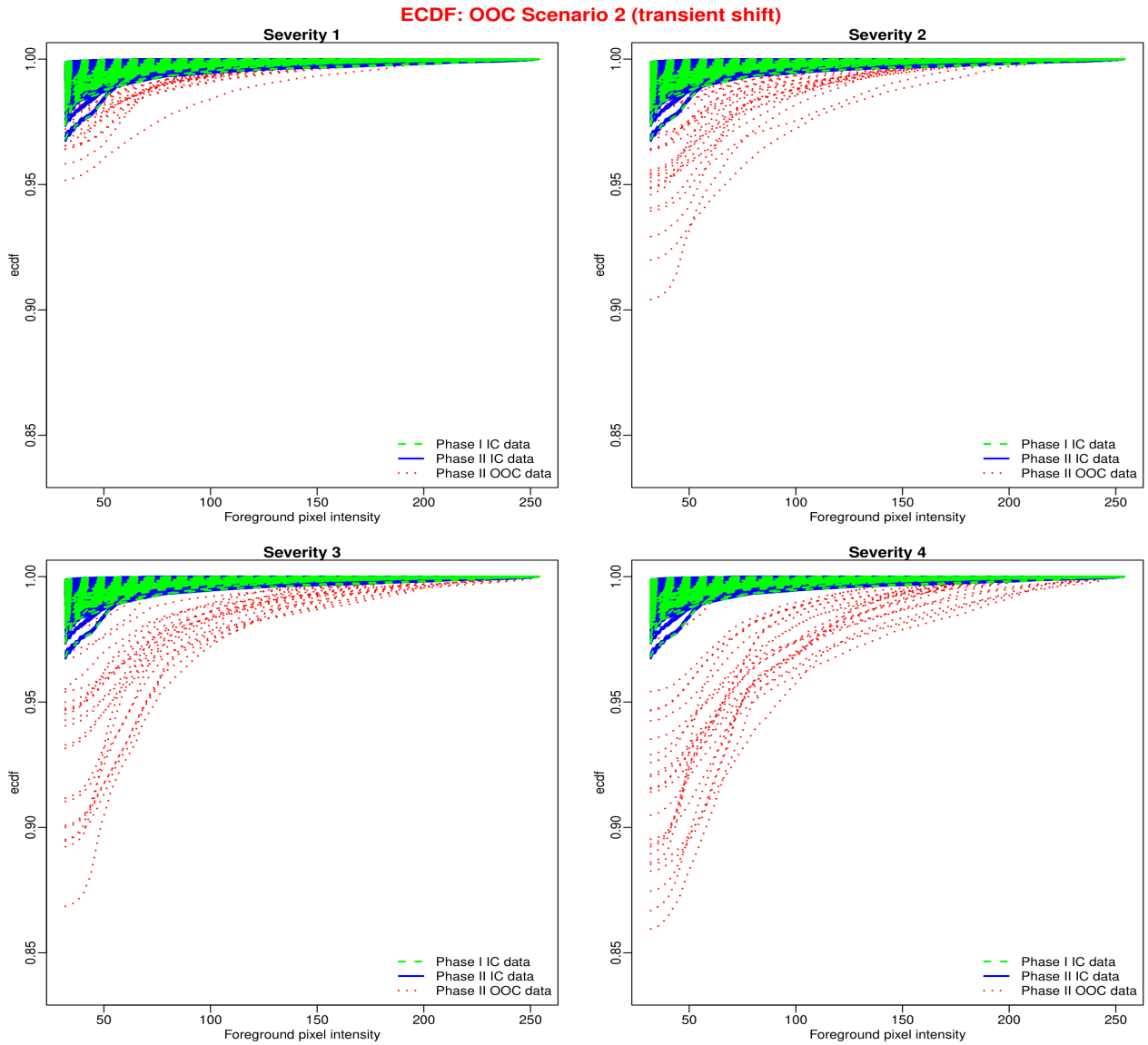

Figure 16: Ecdfs of phase I and phase II video frames in OOC scenario 2 included in the simulated study (different panels refer to different severity levels).

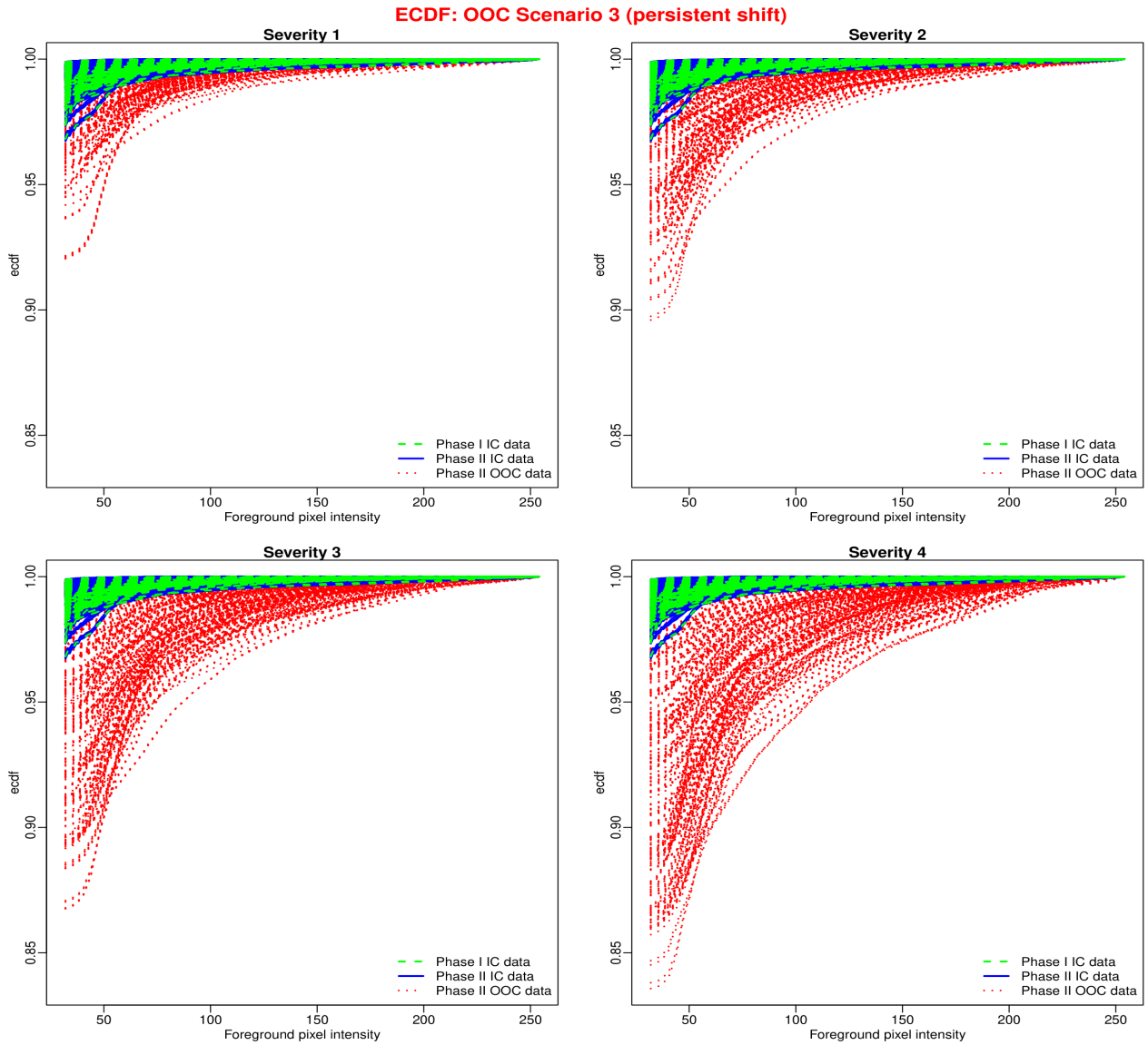

Figure 17: Ecdfs of phase I and phase II video frames in OOC scenario 3 included in the simulated study (different panels refer to different severity levels).

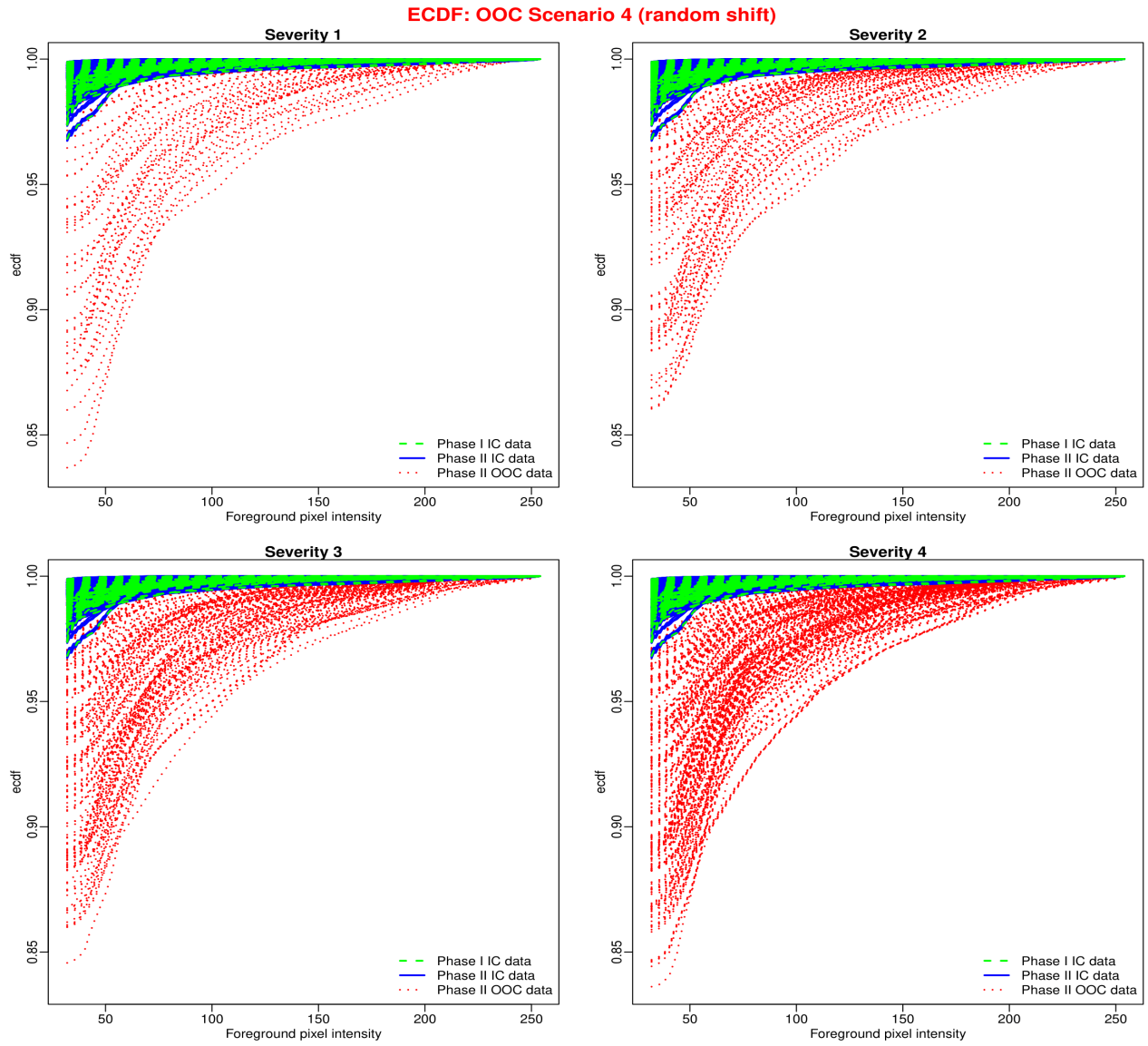

Figure 18: Ecdfs of phase I and phase II video frames in OOC scenario 4 included in the simulated study (different panels refer to different severity levels).